

# Order-Tuned Vibration Absorbers for a Rotating Flexible Structure with Cyclic Symmetry

Brian J. Olson <sup>a,1</sup>, Steven W. Shaw <sup>a</sup>, and Christophe Pierre <sup>b,2</sup>

<sup>a</sup>*Department of Mechanical Engineering, Michigan State University, East Lansing, MI 48824-1226, USA*

<sup>b</sup>*Department of Mechanical Engineering and Applied Mechanics, The University of Michigan, Ann Arbor, MI 48109-2125, USA*

---

## Abstract

This paper investigates the use of order-tuned absorbers to attenuate vibrations of flexible blades in a bladed disk assembly subjected to engine order excitation. The blades are modeled by a cyclic chain of  $N$  oscillators, and a single vibration absorber is fitted to each blade. These absorbers exploit the centrifugal field arising from rotation so that they are tuned to a given order of rotation, rather than to a fixed frequency. A standard change of coordinates based on the cyclic symmetry of the system essentially decouples the governing equations of motion, yielding a closed form solution for the steady-state response of the overall system. These results show that optimal reduction of blade vibrations is achieved by tuning the absorbers to the excitation order  $n$ , but that the resulting system is highly sensitive to small perturbations. Intentional *detuning* (meaning that the absorbers are slightly over- or under-tuned relative to  $n$ ) can be implemented in order to improve the robustness of the design. It is shown that by slightly undertuning the absorbers there are no system resonances over the full range of possible rotor speeds, resulting in a system that is robust to *mistuning* (i.e., small random uncertainties in the system parameters) of the absorbers and/or blades. These results offer a basic understanding of the dynamics of a bladed disk assembly fitted with order-tuned vibration absorbers, and serve as a first step to the investigation of more realistic models, where, for example, imperfections, multi-DOF blade models, nonlinear effects, and general-path absorbers are employed.

*Key words:* order-tuned absorbers, bladed disk, cyclic symmetry, circulant matrix

---

# 1 Introduction

This work investigates the use of order-tuned absorbers to attenuate vibrations in a rotating flexible structure with cyclic symmetry. The applications of interest are turbine blades, bladed disk assemblies, and blisks (integral disk-blade systems), such as might be found in a jet engine. Flow entering an engine invariably meets static obstructions, such as struts, stator vanes, etc., in addition to rotating components, such as fans, compressors, and turbines in its path to the exhaust. Even in steady operation, therefore, the flow slightly upstream of these bladed assemblies is spatially non-uniform in pressure, temperature, and so on. This results in a static force field that varies circumferentially relative to the engine casing and gives rise to traveling wave dynamic loading on the blades—the so-called *engine order excitation*—which is characterized by excitation frequencies that are proportional to the mean rotational speed of the rotor [1]. Such excitations can lead to high cycle fatigue (HCF) failure, noise, reduced performance, and other undesirable effects [2]. This is an ideal setting for the use of centrifugally-driven, order-tuned vibration absorbers, yet their implementation to such systems has received little attention to date. Much is already known about the dynamic behavior of systems of vibration absorbers, and the same is true for systems with symmetries in general and for rotating flexible structures in particular [3, 4]. This work aims to apply the theory, methodology, and design of order-tuned absorbers to such systems.

An important feature of order-tuned absorber systems is that they are tuned to a particular *order* of rotation, and are thus effective over a range of operating speeds, rather than to a particular speed. This is in contrast to the classical *frequency-tuned* absorbers due to Ormondroyd and Den Hartog [5, 6], which are effective only at a particular frequency. The desired *order-tuning* [7] is achieved by exploiting the centrifugal field due to rotation to provide the absorber restoring forces, as opposed to an elastic element. Order-tuned absorbers have been quite successful in rotating machinery applications, where they are used to attenuate torsional vibrations that arise from fluctuating torques acting on the rotor. Some mature applications include light aircraft engines [8] and helicopter rotors [9], and, more recently, diesel camshafts [10] and advanced technology automotive engines [11]. In contrast, here we consider the case where the rotor runs at a constant speed, but flexible attachments experience vibrations due to applied loads. Linear analytical studies of order-tuned absorbers applied to such systems have been carried out, for

---

*Email addresses:* olsonbr1@egr.msu.edu (Brian J. Olson), shawsw@egr.msu.edu (Steven W. Shaw), pierre@umich.edu (Christophe Pierre).

<sup>1</sup> Address all correspondence to this author.

<sup>2</sup> Effective July 1, 2005: Dean, College of Engineering, McGill University, 817 Sherbrooke Street West, Montreal, Quebec H3A 2K6, CANADA.

example, by Hollkamp *et al.* [12], and also Wang *et al.* [13]. Recent experimental work by Duffy and coworkers [14] has demonstrated the effectiveness of the impacting response of such absorbers, and Shaw and Pierre [15] have analytically investigated the response of a single flexible element fitted with an order-tuned impact absorber.

The rotating flexible structures of interest consist of an array of interconnected constituent parts (substructures) whose geometry and structural properties are rotationally periodic, and they are said to have *cyclic symmetry* [16]. In a bladed disk, for example, the fundamental substructure is one blade plus the corresponding segment of the disk, which is collectively referred to as a *sector*. The entire dynamics of these systems can be captured by analyzing a single sector [17, 18], a feature shared by all perfectly cyclic systems. The cyclically symmetric model considered here consists of  $N$  sectors (Fig. 1b), each of which is composed of a single degree-of-freedom (DOF) blade model with an attached absorber. Hence each sector possesses two DOF, and these are coupled such that the overall system (Fig. 1a) has  $2N$  DOF. While it is possible to handle the governing (coupled)  $2N$  equations of motion using the tools from linear vibration theory [19], a standard change of coordinates based on the cyclic symmetry of the system is employed to reduce the problem to  $N$  uncoupled 2-DOF systems [16–18, 20–22]. Not only does this offer substantial computational savings, it also yields closed-form solutions describing the forced response, which clearly shows the effects of the absorbers on the system. The main objective of this work is to investigate the overall system behavior and to assess the effectiveness of the absorbers in attenuating the blade vibrations, especially near resonance. Absorber tuning plays a key role in this analysis.

The cyclicity of the bladed disk model to be considered results in block circulant system matrices. The basic properties of these matrices are outlined in Appendix A, along with other relevant mathematical preliminaries. A detailed account of the theory of circulants can be found in the classical text by Davis [23].

Generally, the blades on a turbomachinery rotor are meant to be identical. In practice, however, there always exist small random uncertainties among the blades due to manufacturing tolerances, in-service wear, and so on. These small variations, or *mistuning*, can have a drastic effect on the forced system response. In particular, they can lead to a confinement of vibration energy to a few blades or even a single blade, a phenomenon known as *localization* [24–26]. Due to this spatial confinement of energy, some of the blades may experience higher amplitudes than what is predicted from the ideal, perfectly periodic system [27–31]. In what follows the model is assumed to be ideal with identical blades and identical absorbers. The effects of mistuning on the absorber performance is left for future work.

The main body of the paper is organized as follows. The system model is described in Section 2 and the dimensionless equations of motion are hence formulated for a single sector in Section 2.1 and subsequently for the overall coupled system in Section 2.2. Two special cases of these governing equations are considered: the case when the blades (resp. absorbers) are locked in their zero positions relative to the rotating hub (resp. blades) in Section 2.3 (resp. Section 2.4). The former motivates the absorber tuning order, which is employed in subsequent sections to tune the absorbers to a given order of the excitation, and the latter is investigated in detail in Section 3.1, with the aim of providing a benchmark against which the effectiveness of the absorbers can be evaluated. The forced response of the general system is detailed in Section 3.2, and an absorber tuning strategy is motivated in Section 4. The paper closes with some concluding remarks and directions for future work in Section 5.

## 2 Mathematical Model

An idealized model of a bladed disk assembly is shown schematically in Fig. 1a. It consists of a cyclic array of  $N$  identical blades, each modeled by a simple pendulum of length  $L$  and mass  $M$ . These are uniformly attached around the periphery of a rigid disk of radius  $H$ , which rotates at a constant speed  $\Omega$  about a fixed axis through  $O$ . The single-mode flexural stiffness of each blade (primary system) is captured by identical linear torsional springs of stiffness  $k_b$ , and the inter-blade coupling (due to shrouds, aerodynamic effects, and so on) is captured by linear springs of stiffness  $k_c$ . The coupling springs connect adjacent blades a distance  $b$  radially along the blades relative to their attachment points to the rotor. It is assumed that the springs are unstressed when the blades are in a purely radial configuration, that is, when  $\theta_i = 0$  for each  $i$  in  $\mathcal{N} = \{1, 2, \dots, N\}$ .

Identical vibration absorbers of mass  $m$  (typically  $m \ll M$ ) are fitted to each blade. They ride on circular paths of radius  $d$  relative to the blades, which are centered a distance  $\alpha L$  ( $\alpha \leq 1$ ) radially along the blade pendulums, and their dynamics are captured by the relative angular coordinates  $\psi_i$  ( $i \in \mathcal{N}$ ). Physically, the absorber angles are limited to some value  $\psi_o$  by stops, which represent the rattling space limits of the turbine blades. Impacts occur whenever  $|\psi_i| = \psi_o$ , the dynamics of which are investigated in [15] for the case of a single isolated blade/absorber combination. In the present analysis it is assumed that  $|\psi_i| < \psi_o$  and  $\theta_i$  are sufficiently small so that the dynamics of the overall system are captured by a linearized model.

There are a number of ways to model the system damping, but in light of the inherently small levels encountered in practice the details are not crucial.

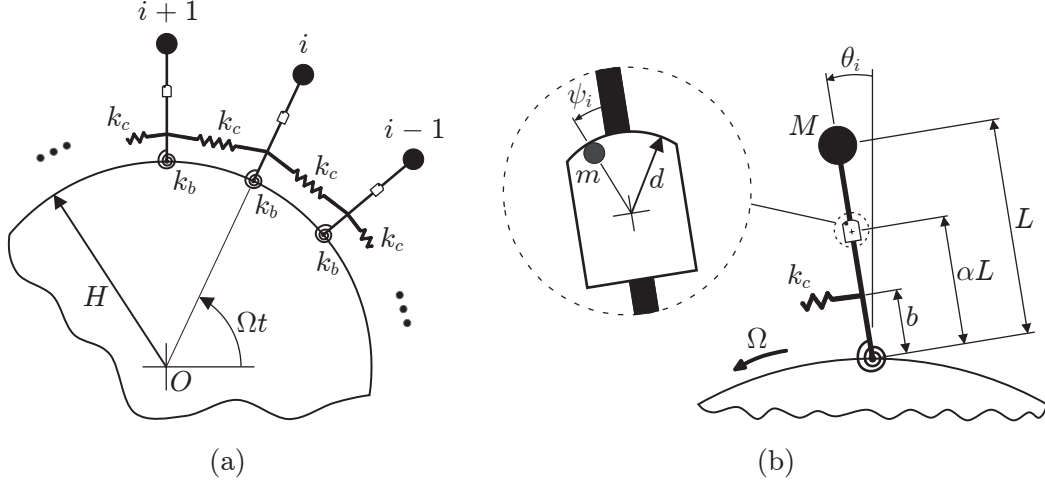


Fig. 1. (a) Model of bladed disk assembly and (b) sector model.

(It is acknowledged that modeling and quantifying these details in actual structural systems and absorber implementations can be quite challenging.) Damping ratios for the structures of interest are typically 0.1% or less relative to critical damping. Moreover, in order to achieve the desired order tuning of the absorbers, the absorber damping is made as small as possible. For the purposes of this study, therefore, it will suffice to employ simple linear viscous damping models; the absorber, blade, and inter-blade damping is captured by linear torsional and translational dampers (not shown in Fig. 1) with constants  $c_a$ ,  $c_b$ , and  $c_c$ , respectively.

The primary systems (blades) are harmonically excited in the transverse sense by engine order (e.o.) excitation of order  $n$ . Consider, for example, an engine in steady operation with  $n$  evenly-spaced obstructions such as stator vanes, struts, etc., upstream of the bladed disk assembly. As discussed in [1], these obstructions produce a circumferential variation in the (mean) axial pressure that is essentially proportional to  $\cos n\theta$ , where  $\theta$  is an angular position measured relative to the engine casing. Thus a blade rotating through this static pressure field experiences a force proportional to  $\cos n\Omega t$ , where  $\Omega$  is the constant angular speed of the bladed disk assembly and  $t$  is time. An adjacent blade experiences the same force, but at a constant fraction of time later. This type of excitation is defined as *engine order excitation of order  $n$* , or  $n$  e.o., and can be modeled by

$$F_i(t) = F_o e^{j\phi_i} e^{jn\Omega t}, \quad i \in \mathcal{N} \quad (1)$$

where  $F_o$  is the strength of the excitation,  $j = \sqrt{-1}$ , and

$$\phi_i = 2\pi \frac{n}{N} (i - 1), \quad i \in \mathcal{N} \quad (2)$$

is the *inter-blade phase angle*. If the phase angle between sector 1 and sector  $i$

is denoted by

$$\varphi_i = \frac{2\pi(i-1)}{N}, \quad i \in \mathcal{N} \quad (3)$$

then the inter-blade phase angle can be written as  $\phi_i = n\varphi_i$ . In the applications of interest the *engine order*  $n$  is a positive integer.<sup>3</sup> Consideration of all possible engine orders can be somewhat cumbersome, however, since one must not only distinguish between odd and even  $n$  in the analysis, and also examine how certain features (e.g. excited modes) alias relative to  $N$  [32]. In order to eliminate some of the unnecessary details, and to focus on an absorber tuning strategy, we thus restrict  $0 < n < N$  (though it is possible for  $n \geq N$  in practice). This does not qualitatively affect the approach nor the conclusions.

The equations of motion for a single sector are developed in the next section and for the overall system in Section 2.2. Two special cases of the governing equations are subsequently considered in which the blades are locked relative to the rotor (Section 2.3) and the absorbers are locked relative to the blades (Section 2.4). The first of these special cases motivates the absorber tuning order, which is used in Section 4 to tune the absorbers to a given order of the excitation. The second special case offers a baseline against which to assess the effectiveness of the absorbers when they are free to move.

## 2.1 Sector Model

The equations of motion for each 2-DOF sector are derived by employing Lagrange's method and are linearized for small motions of the primary and absorber systems, that is, for small  $\theta_i$  and  $\psi_i$ . The resulting linear equations are divided through by the inertia term  $ML^2$  and time is rescaled according to  $\tau = \omega_o t$ , where

$$\omega_o = \sqrt{(k_b/L^2)/M} \quad (4)$$

is the undamped natural frequency of a single isolated blade (without an absorber) with zero coupling ( $k_c = 0$ ) and zero rotor speed ( $\Omega = 0$ ). Then the dynamics of the  $i^{\text{th}}$  sector are governed by

$$\left. \begin{aligned} \mathbf{M}\mathbf{z}_i'' + \mathbf{C}\mathbf{z}_i' + \mathbf{K}\mathbf{z}_i + \mathbf{C}_c \left( -\mathbf{z}'_{i-1} + 2\mathbf{z}'_i - \mathbf{z}'_{i+1} \right) \\ + \mathbf{K}_c \left( -\mathbf{z}_{i-1} + 2\mathbf{z}_i - \mathbf{z}_{i+1} \right) = \mathbf{f} e^{j\phi_i} e^{jn\sigma\tau} \end{aligned} \right\}, \quad i \in \mathcal{N} \quad (5)$$

where

$$\mathbf{z}_i = \begin{bmatrix} x_i \\ y_i \end{bmatrix} = \begin{bmatrix} \theta_i/\psi_o \\ \psi_i/\psi_o \end{bmatrix} \quad (6)$$

<sup>3</sup> The case of noninteger  $n$  is non-physical for bladed disk assemblies under engine order excitation, but it is of academic interest and may be possible in other systems. The case of  $n \in \mathbb{R}_+$  and its implications in cyclic systems is investigated in [22].

Table 1  
Elements of  $\mathbf{M}$ ,  $\mathbf{C}$ , and  $\mathbf{K}$ .

$M_{11} = 1 + \mu(\alpha + \gamma)^2$	$C_{11} = \xi_b$	$K_{11} = 1 + (1 + \mu(\alpha + \gamma)) \delta \sigma^2$
$M_{12} = \mu\gamma(\alpha + \gamma)$	$C_{12} = -\xi_a$	$K_{12} = \mu\gamma\delta\sigma^2$
$M_{21} = M_{12}$	$C_{21} = 0$	$K_{21} = K_{12}$
$M_{22} = \mu\gamma^2$	$C_{22} = \xi_a$	$K_{22} = \mu\gamma(\alpha + \delta)\sigma^2$

is a vector of nondimensional physical coordinates ( $x_i$  and  $y_i$  describe the dynamics of the  $i^{\text{th}}$  blade and absorber, respectively),  $\phi_i$  is the inter-blade phase angle defined by Eq. (2),  $\sigma = \Omega/\omega_o$  is the dimensionless angular speed of the rotor, and  $(\cdot)' = d(\cdot)/d\tau$ . In Eq. (5) the subscripts are taken mod  $N$  here and in subsequent sections such that  $\mathbf{z}_{N+1} = \mathbf{z}_1$  and  $\mathbf{z}_0 = \mathbf{z}_N$ . The elements of the sector mass, damping, and stiffness matrices are given in Table 1, and the attendant dimensionless parameters are defined in Table 2. The matrices

$$\mathbf{C}_c = \begin{bmatrix} \xi_c & 0 \\ 0 & 0 \end{bmatrix}, \quad \mathbf{K}_c = \begin{bmatrix} \nu^2 & 0 \\ 0 & 0 \end{bmatrix}, \quad (7)$$

capture the inter-blade coupling and vanish when  $\xi_c = 0$  and  $\nu = 0$ , respectively, in which case Eq. (5) describes the forced motion of  $N$  isolated blade/absorber systems. (Equation (5) is studied in detail in [15] for the case when  $N = 1$ ,  $\mathbf{K}_c = \mathbf{0}$ , and  $\mathbf{C}_c = \mathbf{0}$ , including the impact dynamics that occur when  $|y_i| = 1$ , that is,  $|\psi_i| = \psi_o$ .) The sector forcing vector is given by

$$\mathbf{f} = \begin{bmatrix} f \\ 0 \end{bmatrix}, \quad (8)$$

where  $f$  is defined in Table 2. Finally, the parameter  $\omega_c = \frac{b}{L}\sqrt{k_c/M}$  (see  $\nu$  in Table 2) is the undamped natural frequency of a single isolated blade (with no absorber) with  $k_b = 0$  and  $\Omega = 0$  and with a single coupling stiffness element  $k_c$  connected to an adjacent, stationary blade.

## 2.2 System Model

By stacking each  $\mathbf{z}_i$  into the configuration vector  $\mathbf{q} = (\mathbf{z}_1, \mathbf{z}_2, \dots, \mathbf{z}_N)^T$ , the governing matrix equation of motion for the overall  $2N$ -DOF system takes the form

$$\hat{\mathbf{M}}\mathbf{q}'' + \hat{\mathbf{C}}\mathbf{q}' + \hat{\mathbf{K}}\mathbf{q} = \hat{\mathbf{f}}e^{jn\sigma\tau}, \quad (9)$$

Table 2

Selected list of dimensionless parameters.

Parameter	Description
$f = F_o L / k_b \psi_o$	Strength of the engine order excitation
$\alpha$	Distance from blade base to absorber base point
$\gamma = d / L$	Length of the absorber pendulum
$\delta = H / L$	Radius of the rotor disk
$\mu = m / M$	Absorber mass
$\nu = \omega_c / \omega_o = \sqrt{\frac{k_c}{k_b / b^2}}$	Inter-blade coupling strength
$\phi_i = 2\pi \frac{n}{N} (i - 1)$	$i^{th}$ inter-blade phase angle
$\tau = \omega_o t$	Time
$\xi_a = \frac{c_a / L^2}{\sqrt{(k_b / L^2) M}}$	Absorber damping constant
$\xi_b = \frac{c_b / L^2}{\sqrt{(k_b / L^2) M}}$	Blade damping constant
$\xi_c = \left(\frac{b}{L}\right)^2 \frac{c_c}{\sqrt{(k_b / L^2) M}}$	Coupling damping constant
$\sigma = \Omega / \omega_o$	Angular speed of the rotor

where  $\hat{\mathbf{M}}$  is block diagonal with diagonal blocks  $\mathbf{M}$  and  $\hat{\mathbf{K}}$  is block circulant with the  $N$  generating matrices  $\mathbf{K} + 2\mathbf{K}_c, -\mathbf{K}_c, \mathbf{0}, \dots, \mathbf{0}, -\mathbf{K}_c$ .<sup>4</sup> The matrix  $\hat{\mathbf{C}}$  is similarly defined by replacing  $\mathbf{K}$  with  $\mathbf{C}$  and  $\mathbf{K}_c$  with  $\mathbf{C}_c$  in  $\hat{\mathbf{K}}$ . In terms of the circulant operator the system mass, damping, and stiffness matrices are given by

$$\left. \begin{aligned} \hat{\mathbf{M}} &= \text{circ}(\mathbf{M}, \mathbf{0}, \mathbf{0}, \dots, \mathbf{0}, \mathbf{0}) = \text{diag}_{i \in \mathcal{N}}(\mathbf{M}) \\ \hat{\mathbf{C}} &= \text{circ}(\mathbf{C} + 2\mathbf{C}_c, -\mathbf{C}_c, \mathbf{0}, \dots, \mathbf{0}, -\mathbf{C}_c) \\ \hat{\mathbf{K}} &= \text{circ}(\mathbf{K} + 2\mathbf{K}_c, -\mathbf{K}_c, \mathbf{0}, \dots, \mathbf{0}, -\mathbf{K}_c) \end{aligned} \right\}, \quad (10)$$

where the  $\text{circ}(\cdot)$  operation is defined in Appendix A. Finally, the system forcing vector is

$$\hat{\mathbf{f}} = \left( \mathbf{f} e^{j\phi_1}, \mathbf{f} e^{j\phi_2}, \dots, \mathbf{f} e^{j\phi_N} \right)^T, \quad (11)$$

where  $\mathbf{f}$  is given by Eq. (8) and  $\phi_i$  is defined by Eq. (2).

<sup>4</sup> See [23] for a comprehensive treatment of circulant matrices and their properties. A brief review of such matrices and other mathematical preliminaries is given in Appendix A.

### 2.3 Special Case: The Blades Locked

Consider the special case when the blades are locked in their zero positions relative to the rotating disk. This leads to a system of dynamically isolated absorbers that oscillate freely under the influence of centrifugal effects. The governing equations follow from Eq. (5) by setting  $x_i = x'_i = x''_i \equiv 0$ , and are given by

$$M_{22}y''_i + C_{22}y'_i + K_{22}y_i = 0, \quad i \in \mathcal{N} \quad (12)$$

where the mass, damping, and stiffness terms  $M_{22}$ ,  $C_{22}$ , and  $K_{22}$  are defined in Table 1. Equation (12) is a set of  $N$  uncoupled and unforced single-DOF harmonic oscillators. Their dimensionless undamped natural frequencies are given by

$$\bar{\omega}_{22} \equiv \frac{\omega_{22}}{\omega_o} = \sqrt{\frac{\alpha + \delta}{\gamma}} \sigma \equiv \tilde{n}\sigma, \quad (13)$$

or  $\omega_{22} = \tilde{n}\Omega$  in dimensional form, where  $\omega_o$  is defined by Eq. (4) and

$$\tilde{n} = \sqrt{\frac{\alpha + \delta}{\gamma}} \quad (14)$$

is defined to be the *absorber tuning order*. Since the absorbers are restrained only through centrifugal effects,  $\bar{\omega}_{22}$  scales directly with  $\sigma$  [12, 14]. This feature is exploited in Section 4 to tune the absorbers to a given *order* of the excitation, rather than to a fixed *frequency*, as is done in the classical sense [6]. The tuning parameter  $\tilde{n}$  is used for this purpose and is determined by selecting the dimensionless curvature of the pendulum absorber  $\gamma$  (dimensionally  $d$ ) and the distance of its effective attachment point from the center of rotation of the rotor, that is,  $\alpha + \delta$  (dimensionally  $\alpha L + H$ ).

### 2.4 Special Case: The Absorbers Locked

Here we consider a model in which the absorbers are locked in their zero positions relative to the blades. By setting  $y_i = y'_i = y''_i \equiv 0$ , the equations of motion for the  $i^{\text{th}}$  sector follow from Eq. (5) and are given by

$$\left. \begin{aligned} M_{11}x''_i + C_{11}x'_i + K_{11}x_i + \xi_c \left( -x'_{i-1} + 2x'_i - x'_{i+1} \right) \\ + \nu^2 \left( -x_{i-1} + 2x_i - x_{i+1} \right) = f e^{j\phi_i} e^{jn\sigma\tau} \end{aligned} \right\}, \quad i \in \mathcal{N} \quad (15)$$

where the mass, damping, and stiffness terms  $M_{11}$ ,  $C_{11}$  and  $K_{11}$  are defined in Table 1 and their attendant parameters are defined in Table 2, along with the terms  $\xi_c$ ,  $\nu$ , and  $f$ . Here, it is understood that  $x_{N+1} = x_1$  and  $x_0 = x_N$ . The governing matrix equation of motion for the overall  $N$ -DOF system is given

by

$$\hat{\mathbf{M}}_{11}\mathbf{x}'' + \hat{\mathbf{C}}_{11}\mathbf{x}' + \hat{\mathbf{K}}_{11}\mathbf{x} = \hat{\mathbf{f}}_{11}e^{jn\sigma\tau}, \quad (16)$$

where  $\mathbf{x} = (x_1, x_2, \dots, x_N)^T$  is a configuration vector. The system forcing vector is

$$\hat{\mathbf{f}}_{11} = (fe^{j\phi_1}, fe^{j\phi_2}, \dots, fe^{j\phi_N})^T, \quad (17)$$

where the  $i^{\text{th}}$  inter-blade phase angle  $\phi_i$  is defined by Eq. (2) and  $f$  is defined in Table 2. Finally, the system matrices are both symmetric and circulant, and they can be represented by

$$\left. \begin{aligned} \hat{\mathbf{M}}_{11} &= \text{circ}(M_{11}, 0, 0, \dots, 0, 0) = \text{diag}(M_{11}) \\ \hat{\mathbf{C}}_{11} &= \text{circ}(C_{11} + 2\xi_c, -\xi_c, 0, \dots, 0, -\xi_c) \\ \hat{\mathbf{K}}_{11} &= \text{circ}(K_{11} + 2\nu^2, -\nu^2, 0, \dots, 0, -\nu^2) \end{aligned} \right\}, \quad (18)$$

where the coupling term  $\xi_c$  is defined in Table 2. In the absence of coupling, that is, when  $\nu = \xi_c \equiv 0$ , the system matrices given by Eq. (18) are all diagonal, and Eq. (16) is a decoupled set of  $N$  harmonically forced, single-DOF oscillators.

We now detail the steady-state forced response of Eq. (16) (with the absorbers locked) and, subsequently, Eq. (9) (with the absorbers free to move). In both cases a coordinate transformation is employed in order to significantly uncouple the governing matrix equations.

### 3 Forced Response

The forced response of the overall system is governed by Eq. (9), which can be handled using standard techniques [19]. Its solution in the steady-state follows in the usual way and is given by

$$\mathbf{q}^{\text{ss}}(\tau) = \hat{\mathbf{Z}}^{-1}\hat{\mathbf{f}}e^{jn\sigma\tau}, \quad (19)$$

where  $\hat{\mathbf{Z}} = \hat{\mathbf{K}} - n^2\sigma^2\hat{\mathbf{M}} + jn\sigma\hat{\mathbf{C}}$  is the system impedance matrix of dimension  $2N \times 2N$ . However, Eq. (19) does not offer any insight into the design and effectiveness of the proposed vibration absorbers, and it also requires computation of  $\hat{\mathbf{Z}}^{-1}$ , which can be quite involved for many bladed disk models. It is well-known that, due to its cyclic symmetry (and in particular due to the circulant structure of the system matrices [23]), Eq. (9) can be decoupled via a modal (unitary) transformation to a set of  $N$  reduced-order models, each with two DOF [16–18, 20–22]. (The reduced-order models have the same number of DOF as an individual sector, in this case two.) Similar statements can be made for Eq. (16), which captures the system dynamics for the special case

when the absorbers are locked in their zero positions relative to the blades. Since the system matrices are circulant for this special case, one can decouple the  $N$ -DOF model to a set of  $N$ , single-DOF systems. A special feature of the uncoupled systems described above is that only mode  $n + 1$  is excited, provided that  $0 < n < N$  is an integer (as shown subsequently). Hence the steady-state response of the overall  $2N$ -DOF (resp.  $N$ -DOF) system described above reduces to the solution of a single, harmonically forced, 2-DOF (resp. single-DOF) system.

In order to provide a benchmark against which the effectiveness of the absorbers can be evaluated, we first consider the forced response of the system when the absorbers are locked relative to the blades. It should be noted that the corresponding analysis could be obtained directly from the more general analysis of Section 3.2. However, it is instructive to introduce the modal transformation in this simpler setting, which clearly demonstrates the essential features of the approach. The forced response of the general system, where the absorbers are free to move, is investigated in Section 3.2 and employs the same methodology. An absorber tuning strategy is motivated in Section 4 based on these results.

### *3.1 Response with the Absorbers Locked*

The purpose of this section is twofold: to demonstrate the essential features of the analysis, a generalization of which is employed in Section 3.2 for the case when the absorbers are free to move, and to review some of the vibration characteristics of linear cyclic systems. Some specific topics include: decoupling of the equations of motion; orthogonality of the modal forcing vector; the steady-state system response; characteristics of the natural frequencies and attendant normal modes (see [1, 17, 33] for further characteristics); and conditions for resonance. The results will also be useful for comparisons when evaluating the effectiveness of the absorbers in subsequent sections. The reader who is familiar with these topics can proceed, with minimal loss of continuity, to Section 3.2.

#### *3.1.1 Modal Analysis*

Consider the forced response of the system in Fig. 1a for the special case when the absorbers are locked in their zero positions relative to the blades. Due to the cyclicity of the model and the corresponding circulant structure of the system matrices given by Eq. (18), one can employ a standard unitary (similarity) transformation to decouple the governing equations of motion. In particular, we wish to apply the result given by Eq. (A.7) of Appendix A to

each of the system matrices. This can be achieved by introducing the change of coordinates<sup>5</sup>

$$\mathbf{x} = \mathbf{E}\tilde{\mathbf{x}}, \quad \text{or} \quad x_i = \mathbf{e}_i^T \tilde{\mathbf{x}}, \quad i \in \mathcal{N} \quad (20)$$

where  $\mathbf{E}$  is the  $N \times N$  complex Fourier matrix and  $\mathbf{e}_i$  is its  $i^{\text{th}}$  column (these are defined by Eq. (A.2) and Eq. (A.3) of Appendix A), and  $\tilde{\mathbf{x}} = (\tilde{x}_1, \tilde{x}_2, \dots, \tilde{x}_N)^T$  is a vector of modal, or *cyclic* coordinates. Substituting Eq. (20) into Eq. (16), multiplying from the left by the unitary matrix  $\mathbf{E}^{\mathcal{H}}$ , and invoking Eq. (A.7) of Appendix A yields a system of  $N$  decoupled scalar equations. They are

$$\tilde{M}_{11}^{(p)} \tilde{x}_p'' + \tilde{C}_{11}^{(p)} \tilde{x}_p' + \tilde{K}_{11}^{(p)} \tilde{x}_p = \mathbf{e}_p^{\mathcal{H}} \hat{\mathbf{f}}_{11} e^{jn\sigma\tau}, \quad p \in \mathcal{N} \quad (21)$$

where  $(\cdot)^{\mathcal{H}} = (\bar{\cdot})^T$  denotes the conjugate transpose and  $\mathbf{e}_p^{\mathcal{H}} \hat{\mathbf{f}}_{11}$  is the  $p^{\text{th}}$  element of  $\mathbf{E}^{\mathcal{H}} \hat{\mathbf{f}}_{11}$ , and is discussed subsequently. The modal mass, damping, and stiffness terms follow from Eq. (A.8) and are given by

$$\left. \begin{aligned} \tilde{M}_{11}^{(p)} &= M_{11} \\ \tilde{C}_{11}^{(p)} &= C_{11} + 2\xi_c(1 - \cos \varphi_p) \\ \tilde{K}_{11}^{(p)} &= K_{11} + 2\nu^2(1 - \cos \varphi_p) \end{aligned} \right\}, \quad p \in \mathcal{N} \quad (22)$$

where  $\varphi_p$  is defined by Eq. (3), the elements  $M_{11}$ ,  $C_{11}$ , and  $K_{11}$  are defined in Table 1, and their attendant parameters are given in Table 2. Note that the identity  $w^{(p-1)} + w^{(N-1)(p-1)} = 2 \cos \varphi_p$  has been employed, where  $w = e^{\frac{2j\pi}{N}}$  is the primitive  $N^{\text{th}}$  root of unity.

Assuming harmonic motion, the  $p^{\text{th}}$  steady-state modal response follows easily from Eq. (21) and is given by

$$\tilde{x}_p^{\text{ss}}(\tau) = \frac{1}{\tilde{\Gamma}_{11}^{(p)}} \mathbf{e}_p^{\mathcal{H}} \hat{\mathbf{f}}_{11} e^{jn\sigma\tau}, \quad p \in \mathcal{N} \quad (23)$$

where

$$\tilde{\Gamma}_{11}^{(p)} = \tilde{K}_{11}^{(p)} - n^2 \sigma^2 \tilde{M}_{11}^{(p)} + jn\sigma \tilde{C}_{11}^{(p)}, \quad p \in \mathcal{N}. \quad (24)$$

Under the assumption that  $0 < n < N$  is an integer, the  $p^{\text{th}}$  modal forcing

<sup>5</sup> The reader who is not familiar with transformations of this type should regard Eq. (20) as the usual modal transformation employed in elementary linear vibration theory. The columns  $\mathbf{e}_i$  of the fourier matrix  $\mathbf{E}$  are, in fact, the eigenvectors of *any* circulant matrix, and hence they define the system mode shapes for *all* linear cyclic systems with a single DOF per sector.

term simplifies considerably and is given by [16, 17, 22]

$$\begin{aligned} \mathbf{e}_p^{\mathcal{H}} \hat{\mathbf{f}}_{11} &= \frac{f}{\sqrt{N}} \sum_{k=1}^N w^{(k-1)(n+1-p)} \\ &= \begin{cases} \sqrt{N} f, & p = n + 1 \\ 0, & \text{otherwise} \end{cases} \end{aligned} \quad (25)$$

Equation (25) shows that only mode  $n + 1$  is excited and, therefore,<sup>6</sup>

$$\tilde{x}_{n+1}^{\text{ss}}(\tau) = \frac{\sqrt{N} f}{\tilde{\Gamma}_{11}^{(n+1)}} e^{jn\sigma\tau} \quad (26)$$

is the only non-zero modal response in the steady-state. The response of sector  $i$  (in physical coordinates) follows from the transformation given by Eq. (20) and is given by  $x_i^{\text{ss}} = \mathbf{e}_i^T \tilde{\mathbf{x}}^{\text{ss}}$ , or

$$x_i^{\text{ss}}(\tau) = X e^{j\phi_i} e^{jn\sigma\tau}, \quad i \in \mathcal{N} \quad (27)$$

where  $\tilde{\mathbf{x}}^{\text{ss}}(\tau) = (0, \dots, 0, \tilde{x}_{n+1}^{\text{ss}}(\tau), 0, \dots, 0)^T$  and  $w^{n(i-1)} = e^{j\phi_i}$  have been employed and  $X = f / \tilde{\Gamma}_{11}^{(n+1)}$  is the steady-state amplitude of the blades. Equation (27) shows that each blade behaves identically except for a constant phase shift from one sector to another, which is captured by the inter-blade phase angle  $\phi_i$ . This approach offers a significant computational advantage over the brute force solution of the full  $N$ -DOF system, and it is employed in Section 3.2 for the general case when the absorbers are free to move.

### 3.1.2 Eigenfrequency Characteristics and Conditions for Resonance

Since the transformation given by Eq. (20) is unitary, the (dimensionless) natural frequencies  $\bar{\omega}_{11}^{(i)}$  are preserved and they follow in the usual way from  $\tilde{K}_{11}^{(i)}$  and  $\tilde{M}_{11}^{(i)}$ . In terms of the parameters defined in Table 2, they are given by

$$\bar{\omega}_{11}^{(i)} \equiv \frac{\omega_{11}^{(i)}}{\omega_o} = \sqrt{\frac{1 + \delta\sigma^2(1 + \mu(\alpha + \gamma)) + 2\nu^2(1 - \cos\varphi_i)}{1 + \mu(\alpha + \gamma)^2}}, \quad i \in \mathcal{N} \quad (28)$$

<sup>6</sup> It is customary in the rotordynamics literature to designate the system modes in terms of their ‘‘diamatral components.’’ Specifically, if  $0 < n \leq N/2$  (or  $0 < n \leq (N - 1)/2$  if  $N$  is odd) then an  $n$  e.o excitation can only excite modes with  $n$  ‘‘nodal diameters’’. However, such a designation is slightly more cumbersome if one considers larger values of  $n$  (in this work we consider  $0 < n < N$ ) and hence we shall say instead that an engine order  $n$  excites only mode  $p = n + 1$ .

where  $\omega_o$  is given by Eq. (4) and  $\varphi_i$  is defined by Eq. (3). For zero inter-blade coupling ( $\nu = 0$ ) all of the natural frequencies are identical, and they increase with increasing rotor speed  $\sigma$  due to centrifugal effects. The presence of the absorber masses ( $\mu \neq 0$ ) slightly lowers the natural frequencies. For very small absorber masses relative to the mass of the blades, that is,  $0 < \mu \ll 1$ , the natural frequencies can be approximated by

$$\bar{\omega}_{11}^{(i)} \cong \sqrt{1 + \delta\sigma^2 + 2\nu^2(1 - \cos \varphi_i)}, \quad i \in \mathcal{N} \quad (29)$$

which clearly exhibits the centrifugal stiffening effects of the primary systems and also the effect of the coupling. Finally, if  $\mu = \nu = \sigma \equiv 0$  we recover  $\bar{\omega}_{11}^{(i)} = 1$ , or  $\omega_{11}^{(i)} = \omega_o$ , which was used in Section 2.1 to nondimensionalize the model.

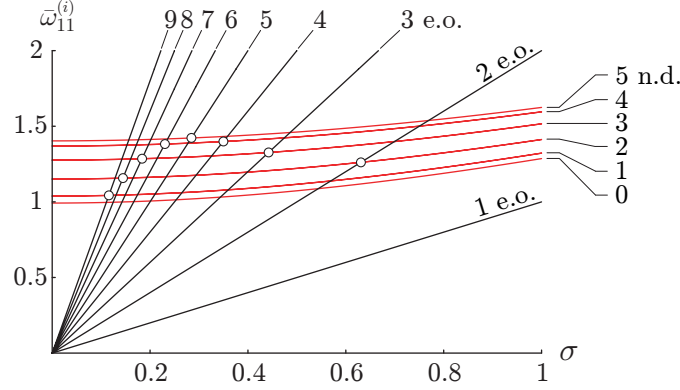
It is clear that there will be repeated natural frequencies due to the cosine term in Eq. (28), and in particular since  $\cos \varphi_i = \cos \varphi_{N+2-i}$  (for appropriate values of  $i$ ), a feature shared by all linear cyclic systems with nearest-neighbor coupling. This degeneracy of the eigenfrequencies is due to the structure of  $\hat{\mathbf{K}}_{11}$ , which has the form  $\text{circ}(a, b, 0, \dots, 0, b)$ , and is manifest in the cyclic term

$$1 - \cos \varphi_i = 1 - \cos\left(\frac{2\pi(i-1)}{N}\right) \quad (30)$$

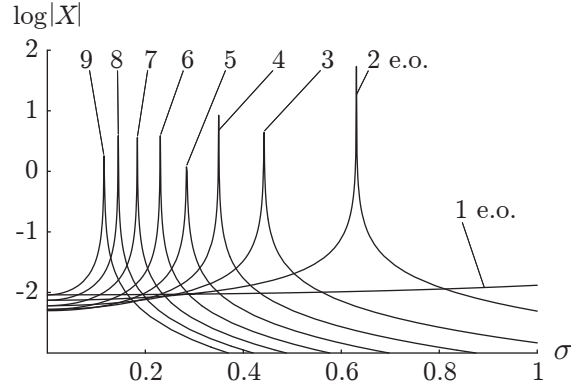
in the modal stiffness matrix of Eq. (22), and hence in the corresponding natural frequencies. The natural frequency corresponding to  $i = 1$  (zero harmonic of Eq. (30)) is distinct, but the remaining natural frequencies appear in repeated pairs, except for the case of even  $N$ , in which case the  $i = (N + 2)/2$  frequency ( $N/2$  harmonic) is also distinct. There are  $(N - 2)/2$  such pairs if  $N$  is even and  $(N - 1)/2$  pairs if  $N$  is odd.

In the turbomachinery literature it is common to plot the natural frequencies in terms of the “diametral components,” that is, the number of “nodal diameters” (n.d.) in their attendant mode shapes [34]. However, in light of the crucial role centrifugal stiffening plays in the absorber performance (this is investigated in Section 4), we shall opt instead for an interference, or *Campbell diagram* representation of the natural frequencies. Such a diagram is shown in Fig. 2a for  $N = 10$  blades and for a particular sector model. In this figure, the natural frequency loci are plotted in terms of the dimensionless rotor speed, and they are seen to increase for increasing  $\sigma$  due to centrifugal effects. The diametral component of each frequency locus is also indicated.

In general, there may be a system resonance whenever  $n\sigma = \bar{\omega}_{11}^{(i)}(\sigma)$  or, equivalently,  $n\Omega = \omega_{11}^{(i)}(\Omega)$ , and these possible resonances can be identified by the intersections of the natural frequency loci with the engine order lines  $n\sigma$  in Fig. 2a. Such resonances can arise, for example, from excitations with multiple dominant orders, mistuning [1], or nonlinear effects. However, for linear cyclic systems, and in the absence of parameter mistuning, an engine order  $n$  (with



(a) Campbell Diagram



(b) Frequency Response Curves

Fig. 2. (a) Campbell diagram for  $N = 10$ ,  $\alpha = 0.84$ ,  $\delta = 0.67$ ,  $\gamma = 0.169$ ,  $\mu = 0.015$ ,  $\nu = 0.5$ , and engine orders (e.o.)  $n = 1, 2, \dots, N - 1$  and (b) the corresponding frequency response curves with  $f = 0.01$ , and  $\xi_b = \xi_c = 0$ .

$0 < n < N$ ) excites only mode  $p = n + 1$ , which is clear from Eq. (25).<sup>7</sup> This is shown in Fig. 2b, which is a plot of the frequency response curves for  $f = 0.01$ ,  $\xi_b = \xi_c = 0$ , and for various engine orders  $n$ . The corresponding intersections of  $n\sigma$  and  $\bar{\omega}_{11}^{(n+1)}(\sigma)$  are indicated by the circles in Fig. 2a. The resonant frequency for the  $n = 3$  case is indicated in Table 3, along with other data corresponding to Fig. 3 and Fig. 4; these are explained in Section 3.2.2 and Section 4.2, respectively.

### 3.2 Response of the General System

We now turn to the forced dynamics of the overall  $2N$ -DOF system, which are governed by Eq. (9), and employ an approach similar to that of Section 3.1.1. In the present case the system matrices  $\tilde{\mathbf{M}}$ ,  $\tilde{\mathbf{C}}$ , and  $\tilde{\mathbf{K}}$  are *block* circulant, and one can (block) decouple these equations to a set of  $N$ , 2-DOF forced

<sup>7</sup> See [32] for a description of the resonance structure for the case when  $n \geq N$ .

Table 3

Data to accompany Figs. 2–4 for a model with  $N = 10$ ,  $n = 3$ ,  $\alpha = 0.84$ ,  $\delta = 0.67$ ,  $\mu = 0.015$ , and  $\xi_a = \xi_b = \xi_c = 0$ . Then  $\beta_{\text{cr}} = -0.00701$  (from Eq. (B.2) of Appendix B) and  $\beta_{\text{cr}}^{\text{app}} = -0.00706$  (from Eq. (49) of Section 4.2).

Fig.	Tuning	$\beta$	$\gamma$	$\tilde{n}$	$\hat{n}$	$\hat{n}_{\text{app}}$	$\nu$	$\sigma_{\text{res}}$
2	–	–	0.169	–	–	–	0.50	0.442
3a	Over	+0.15	0.127	3.45	3.473	3.487	0.01	0.338
3b	Over	+0.15	0.127	3.45	3.473	3.487	0.25	0.364
3c	Over	+0.15	0.127	3.45	3.473	3.487	0.50	0.443
4a	Over	+0.10	0.139	3.3	3.322	3.335	0.50	0.429
–	Exact	0	0.168	3	3.021	3.032	0.50	–
4b	Under	–0.00351	0.169	2.989	3.011	3.021	0.50	–
4c	Under	–0.10	0.207	2.7	2.720	2.729	0.50	0.461

oscillators by employing the result given by Eq. (A.9) of Appendix A.<sup>8</sup>

### 3.2.1 Modal Analysis

We introduce the change of coordinates

$$\mathbf{q} = (\mathbf{E} \otimes \mathbf{I})\mathbf{u}, \quad \text{or} \quad \mathbf{z}_i = (\mathbf{e}_i^T \otimes \mathbf{I})\mathbf{u}, \quad i \in \mathcal{N} \quad (31)$$

where  $\mathbf{E}$  is the  $N \times N$  complex Fourier matrix and  $\mathbf{e}_i$  is its  $i^{\text{th}}$  column,  $\otimes$  is the Kronecker product (these are defined in Appendix A),  $\mathbf{I}$  is the  $2 \times 2$  identity matrix (the dimension of  $\mathbf{I}$  corresponds to the number of DOF in each sector), and  $\mathbf{u} = (\mathbf{u}_1, \mathbf{u}_2, \dots, \mathbf{u}_N)^T$  is a vector of modal, or *cyclic coordinates*  $\mathbf{u}_i = (\tilde{x}_i, \tilde{y}_i)^T$ . Substituting Eq. (31) into Eq. (9) and multiplying from the left by the unitary matrix  $(\mathbf{E} \otimes \mathbf{I})^{\mathcal{H}} = (\mathbf{E}^{\mathcal{H}} \otimes \mathbf{I})$  yields a system of  $N$  block decoupled equations, each with two DOF. They are given by

$$\tilde{\mathbf{M}}_p \mathbf{u}_p'' + \tilde{\mathbf{C}}_p \mathbf{u}_p' + \tilde{\mathbf{K}}_p \mathbf{u}_p = (\mathbf{e}_p^{\mathcal{H}} \otimes \mathbf{I}) \hat{\mathbf{f}} e^{jn\sigma\tau}, \quad p \in \mathcal{N} \quad (32)$$

where  $(\mathbf{e}_p^{\mathcal{H}} \otimes \mathbf{I}) \hat{\mathbf{f}}$  is the  $p^{\text{th}}$   $2 \times 1$  block of  $(\mathbf{E}^{\mathcal{H}} \otimes \mathbf{I}) \hat{\mathbf{f}}$ . The  $2 \times 2$  mass, damping, and stiffness matrices associated with the  $p^{\text{th}}$  mode follow from Eq. (A.10) of Appendix A and are given by

$$\left. \begin{aligned} \tilde{\mathbf{M}}_p &= \mathbf{M} \\ \tilde{\mathbf{C}}_p &= \mathbf{C} + 2\mathbf{C}_c(1 - \cos \varphi_p) \\ \tilde{\mathbf{K}}_p &= \mathbf{K} + 2\mathbf{K}_c(1 - \cos \varphi_p) \end{aligned} \right\}, \quad p \in \mathcal{N} \quad (33)$$

<sup>8</sup> The number of DOF in each decoupled system is that of an individual sector, in this case two.

where  $\varphi_p$  is defined by Eq. (3), the elements of  $\mathbf{M}$ ,  $\mathbf{C}$ , and  $\mathbf{K}$  are defined in Table 1 and their attendant parameters are given in Table 2, and the coupling matrices  $\mathbf{C}_c$  and  $\mathbf{K}_c$  are defined by Eq. (7). In light of Eq. (25), the  $p^{\text{th}}$  modal forcing vector takes the form

$$\begin{aligned} (\mathbf{e}_p^{\mathcal{H}} \otimes \mathbf{I}) \hat{\mathbf{f}} &= \begin{bmatrix} \mathbf{e}_p^{\mathcal{H}} \hat{\mathbf{f}}_{11} \\ 0 \end{bmatrix} \\ &= \begin{cases} \sqrt{N} \mathbf{f}, & p = n + 1 \\ \mathbf{0}, & \text{otherwise} \end{cases} \end{aligned} \quad (34)$$

where  $\hat{\mathbf{f}}_{11}$  is the system forcing vector for the case when the absorbers are locked in their zero positions relative to the blades (Eq. (17)),  $\mathbf{f} = (f, 0)^T$  is the sector forcing vector (Eq. (8)), and  $\mathbf{0} = (0, 0)^T$ . Since only mode  $p = n + 1$  is excited,  $\mathbf{u}_{n+1}(\tau)$  is the only nonzero modal response in the steady-state.

Assuming harmonic motion, and in light of Eq. (34), the  $p^{\text{th}}$  steady-state modal response follows easily from Eq. (32) and is given by

$$\mathbf{u}_p^{\text{ss}}(\tau) = \begin{cases} \sqrt{N} \tilde{\mathbf{Z}}_{n+1}^{-1} \mathbf{f} e^{jn\sigma\tau}, & p = n + 1 \\ \mathbf{0}, & \text{otherwise} \end{cases} \quad (35)$$

where

$$\tilde{\mathbf{Z}}_p = \tilde{\mathbf{K}}_p - n^2 \sigma^2 \tilde{\mathbf{M}}_p + jn\sigma \tilde{\mathbf{C}}_p, \quad p \in \mathcal{N} \quad (36)$$

is the  $p^{\text{th}}$  modal impedance matrix. The response of sector  $i$  (in physical coordinates) follows from the transformation given by Eq. (31) with  $\mathbf{u}^{\text{ss}}(\tau) = (\mathbf{0}, \dots, \mathbf{0}, \mathbf{u}_{n+1}^{\text{ss}}(\tau), \mathbf{0}, \dots, \mathbf{0})^T$  and is given by

$$\mathbf{z}_i^{\text{ss}}(\tau) = \tilde{\mathbf{Z}}_{n+1}^{-1} \mathbf{f} e^{j\phi_i} e^{jn\sigma\tau}, \quad i \in \mathcal{N} \quad (37)$$

where  $w^{n(i-1)} = e^{j\phi_i}$  has been employed. From Eq. (37) it is clear that each blade/absorber combination behaves identically except for a constant phase shift from one sector to another, which is captured by the inter-blade phase angle  $\phi_i$ . This approach offers a significant computational advantage over the brute-force solution to the full  $2N$ -DOF system, as given by Eq. (19).

### 3.2.2 Eigenfrequency Structure and Conditions for Resonance

The  $2N$  dimensionless natural frequencies of the system are defined implicitly by the characteristic polynomial

$$\det(\hat{\mathbf{K}} - \bar{\omega}^2 \hat{\mathbf{M}}) = 0,$$

the solution of which can be quite involved for any reasonable bladed disk model. This effort can be significantly reduced, however, by instead using the modal matrices defined by Eq. (33). We recall that each  $\tilde{\mathbf{M}}_p$  and  $\tilde{\mathbf{K}}_p$  follow from a unitary (similarity) transformation of  $\hat{\mathbf{M}}$  and  $\hat{\mathbf{K}}$  and hence the system natural frequencies are preserved. These eigenfrequencies follow from the  $N$ , second-order characteristic polynomials  $\det(\tilde{\mathbf{K}}_p - \bar{\omega}^2 \tilde{\mathbf{M}}_p) = 0$ , or

$$\det(\mathbf{K} - \bar{\omega}^2 \mathbf{M} + 2\mathbf{K}_c(1 - \cos \varphi_i)) = 0, \quad i \in \mathcal{N} \quad (38)$$

where the sector mass, stiffness, and coupling matrices are defined in Table 1 and by Eq. (7). Equation (38) features the same cyclic term, i.e., Eq. (30), that was encountered in Section 3.1.2 and we thus expect similar eigenfrequency characteristics to the ones described therein. If  $P$  is the number of DOF in an individual sector (in the present study  $P = 2$ ), then there are  $P$  natural frequencies  $\bar{\omega}^{(i)}$  corresponding to each  $i \in \mathcal{N}$ . There are, in this case,  $N$  such groups of  $P = 2$  natural frequencies of the overall system. The multiplicity of these *groups* of natural frequencies is identical to that of the *individual* eigenfrequencies described in Section 3.1.2.

If  $\mathbf{v}_p$  is an eigenvector of the  $p^{\text{th}}$  decoupled modal system, then the corresponding normal mode of the overall system is  $\mathbf{e}_p \otimes \mathbf{v}_p$ , where  $\mathbf{e}_p$  is the  $p^{\text{th}}$  modal vector for the case when the absorbers are locked relative to the blades.<sup>9</sup> With the exception of the  $p = 1$  mode,  $\mathbf{v}_p$  is influenced by the overall system configuration, and in particular by its elastic coupling, which is clear by inspection of the modal stiffness matrices  $\tilde{\mathbf{K}}_p$ . In a particular mode of vibration, the blade and absorber in each sector oscillate either in phase or out of phase relative to one another with amplitudes that depend on the strength and nature of the inter-sector coupling, and these features are captured by  $\mathbf{v}_p$ . The dynamics of each sector are identical, except for a constant difference in phase from one sector to another, and this is captured by  $\mathbf{e}_p$ . Hence the modal configuration of the overall system is described by a composite of these two vectors, which is mathematically given by  $\mathbf{e}_p \otimes \mathbf{v}_p$ .

The  $2N$  dimensionless natural frequencies  $\bar{\omega}_{1,2}^{(i)}$  ( $i \in \mathcal{N}$ ) are plotted in Fig. 3 in terms of the rotor speed  $\sigma$  for  $N = 10$ ,  $n = 3$ , for a particular sector model, and for various levels of the inter-blade coupling  $\nu$ . (The natural frequencies  $\bar{\omega}_{11}^{(i)}$  and  $\bar{\omega}_{22}$  are also shown for reasons discussed below.) In these Campbell diagrams, the  $N$  natural frequencies  $\bar{\omega}_1^{(i)}$  branching from  $\sigma = 0$  (since  $N$  is even there are  $(N - 2)/2 = 4$  repeated pairs) correspond to in-phase modes, wherein the absorber/blade combination in a particular sector oscillates in

<sup>9</sup> When the absorbers are locked each of the the system matrices is a circulant. Since *all* circulant matrices share the same linearly independent eigenvectors, which are the columns of the Fourier matrix (see Appendix A), the system normal modes are  $\mathbf{e}_p$  with  $p \in \mathcal{N}$ .

phase. The remaining  $N$  natural frequencies  $\bar{\omega}_2^{(i)}$  have the same number of repeated pairs and correspond to out-of-phase modes. As shown in Fig. 3a, the frequencies  $\bar{\omega}_1^{(i)}$  and also  $\bar{\omega}_2^{(i)}$  are nearly coincident when the inter-blade coupling is weak, that is, when  $\nu$  is small and they spread out for increasing  $\nu$ , which is shown in Fig. 3b and Fig. 3c. In the absence of inter-blade coupling,  $\bar{\omega}_1^{(i)}$  are identically coincident (as are  $\bar{\omega}_2^{(i)}$ ) and there are exactly  $P = 2$  distinct natural frequencies, each with multiplicity  $N$ .

The frequency loci of Fig. 3 exhibit the classical eigenvalue veering phenomenon, or mutual repulsion of the eigenfrequencies [35, 36]. To see this, we focus on Fig. 3a, where the sets of frequencies  $\bar{\omega}_1^{(i)}$  and  $\bar{\omega}_2^{(i)}$  are mutually nearly coincident. This plot also shows the natural frequencies  $\bar{\omega}_{11}^{(i)}$  (resp.  $\bar{\omega}_{22}$ ), corresponding to the case when the absorbers (resp. blades) are locked relative to the blades (resp. rotor). As the rotor speed  $\sigma$  is increased from zero, the natural frequencies  $\bar{\omega}_1^{(i)}$  (resp.  $\bar{\omega}_2^{(i)}$ ) initially lie close to  $\bar{\omega}_{22} = \tilde{n}\sigma$  (resp.  $\bar{\omega}_{11}^{(i)}$ ), where the absorber tuning order  $\tilde{n}$  is defined by Eq. (14). (For zero rotor speed  $\bar{\omega}_1^{(i)}$  and  $\bar{\omega}_{22}$  are, in fact, coincident and each has the same initial slope of  $\tilde{n}$ .) They exhibit veering near the intersections of  $\bar{\omega}_{11}^{(i)}$  and  $\bar{\omega}_{22}$ , and for large rotor speeds the eigenfrequencies  $\bar{\omega}_1^{(i)}$  asymptotically approach  $\bar{\omega}_{11}^{(i)}$  for each  $i \in \mathcal{N}$ . However, the frequencies  $\bar{\omega}_2^{(i)}$  nearly track  $\bar{\omega}_{22} = \tilde{n}\sigma$  as  $\sigma$  becomes increasingly large, but with a slight offset in slope. This is shown in the inset of Fig. 3a. In fact, it can be shown that

$$\bar{\omega}_2^{(i)} \rightarrow \hat{n}\sigma \quad \text{as} \quad \sigma \rightarrow \infty, \quad (39)$$

where the *critical absorber tuning order*  $\hat{n}(\tilde{n}) > \tilde{n}$  is defined by Eq. (B.1) in Appendix B. This is a crucial observation, one that is exploited in the absorber tuning of Section 4. Finally, note that there is a fixed relationship between  $\tilde{n}$  and  $\hat{n}$ , which is nearly linear for  $\tilde{n} > 1$ . Once the absorber mass  $\mu$  and its tuning order  $\tilde{n}$  are prescribed, then the critical tuning order is automatically set and can be approximated by

$$\hat{n}_{\text{app}} = (1 + \alpha^2 \mu) \tilde{n}, \quad (40)$$

which works quite well for  $\tilde{n} > 1$  and for reasonable choices of  $\alpha$  and  $\mu$ .

Possible resonances can be identified in Fig. 3 by the intersections of the eigenfrequency loci  $\bar{\omega}_{1,2}^{(i)}(\sigma)$  with the order line  $n\sigma$ , and they correspond to rotor speeds  $\sigma = \sigma_{\text{res}}$  for which  $n\sigma = \bar{\omega}_{1,2}^{(i)}(\sigma)$ . However, it was shown in Section 3.2.1 that only mode  $n + 1$  is excited in the steady-state, and hence there will be a system resonance only when

$$n\sigma = \bar{\omega}_{1,2}^{(n+1)}(\sigma), \quad \text{or, equivalently} \quad n\Omega = \omega_{1,2}^{(n+1)}(\Omega) \quad (41)$$

is satisfied. These resonances are indicated by circles in Fig. 3 and they are summarized in Table 3 along with other relevant data. The main objective of

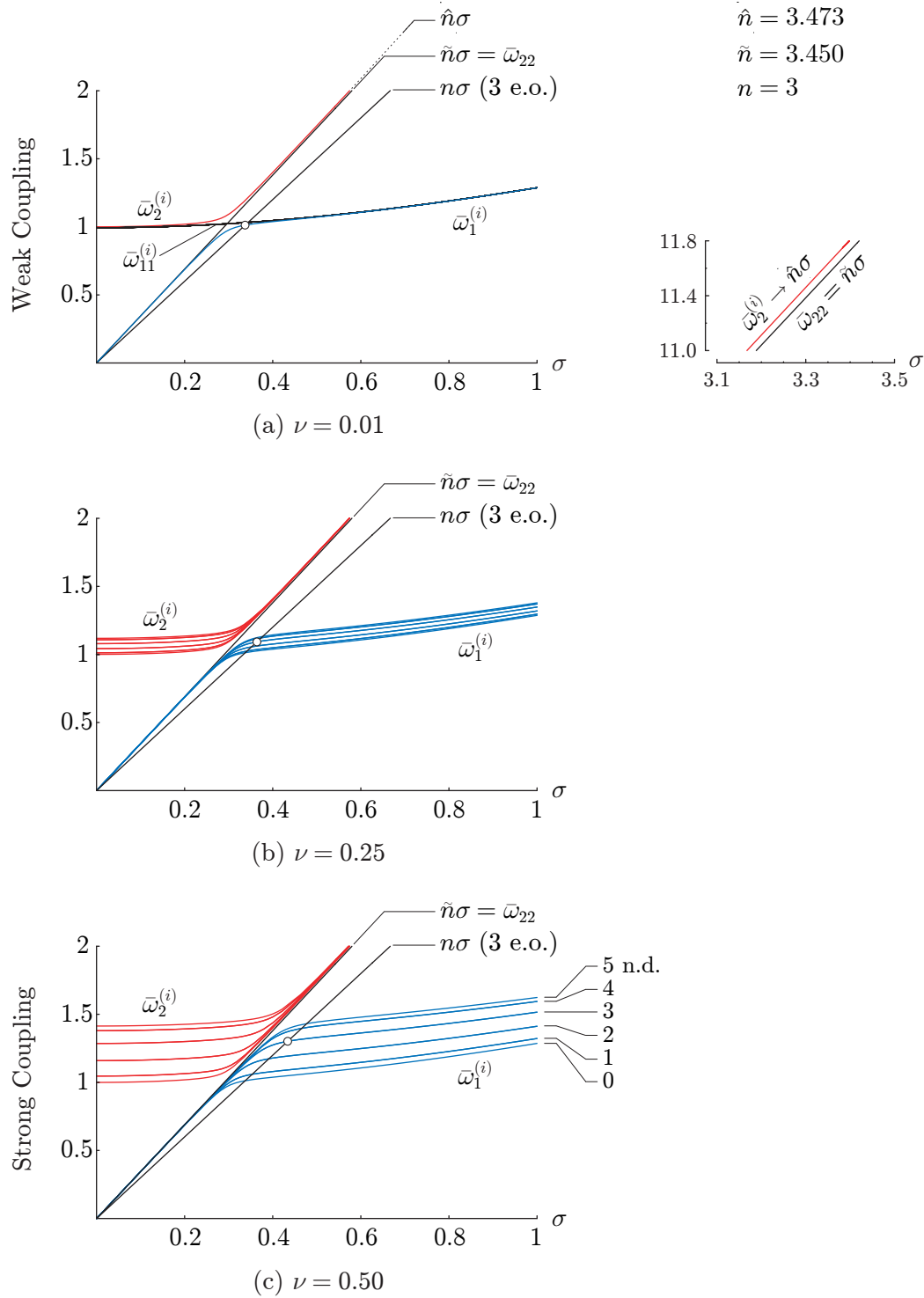


Fig. 3. Campbell diagrams showing the engine order (e.o.) line  $n\sigma$  and the dimensionless natural frequencies  $\bar{\omega}_{11}^{(i)}$ ,  $\bar{\omega}_{22} = \tilde{n}\sigma$ , and  $\bar{\omega}_{1,2}^{(i)}$  versus the dimensionless rotor speed  $\sigma$  for  $N = 10$ ,  $n = 3$ ,  $\alpha = 0.84$ ,  $\gamma = 0.127$ ,  $\delta = 0.67$ , and  $\mu = 0.015$  with: (a)  $\nu = 0.01$ ; (b)  $\nu = 0.25$ ; (c)  $\nu = 0.5$ .

this work is to select the absorber parameters to avoid such resonances over a range of rotor operating speeds; this is the subject of the next section.

As a final note, the inter-blade coupling  $\nu$  is generally quite small, typically on the order of 1%. However, in order to show clearly which modes are excited, and also the effects of absorber (de)tuning, a rather large (unrealistic) value of the coupling will be employed in the ensuing numerical analysis; this does not qualitatively affect the approach nor the conclusions.

## 4 Absorber Tuning

Absorber tuning refers to a particular choice of absorber parameters to attenuate, as much as possible, the response of the primary systems (blades) over a range of operating speeds, and in particular near resonance. This is done by prescribing the dimensionless parameters  $\mu$ ,  $\gamma$ , and  $\alpha$ , which in turn specify the absorber mass  $m$ , the radius of its path  $r$ , and its placement along the blades, respectively. It is shown in Section 4.1 that, in the absence of damping, there exists an absorber tuning such that full annihilation of the blade vibrations is possible, although this may require large-amplitude vibrations of the absorbers. This tuning is accomplished by matching the order of the isolated absorbers to that of the excitation, just as is done with frequencies in the classical dynamic vibration absorber [6], and also with orders for the centrifugal pendulum vibration absorber [7]. In the presence of small absorber damping, however, it becomes impossible to eliminate the blade vibrations completely, and the situation becomes more complicated.<sup>10</sup> The effects of *detuning*<sup>11</sup> the absorbers relative to the excitation order is explored in Section 4.2. It is shown that overtuning the absorbers results in only one system resonance over all possible rotation speeds, even though there are two DOF per sector and there are  $N$  such sectors, and the same is true for most values of undertuning. However, there exists a small region of absorber undertuning, bounded on one side by the exact tuning (zero detuning), for which there are no system resonances. This *no-resonance gap* motivates a particular tuning strategy, which offers a significant reduction of the blade amplitudes and is robust to random perturbations of the system model.

---

<sup>10</sup> An analysis of the damped system is underway and will be considered in a future paper [37].

<sup>11</sup> In this work *detuning* means that all absorbers are identically over- or undertuned relative to  $n$ . This is not to be confused with *mistuning*, which refers to small random uncertainties in the system parameters. In the turbomachinery literature, detuning and mistuning are often used interchangeably, but they must be clearly distinguished in this investigation.

Consider again the Campbell diagrams in Fig. 3. Whereas  $n$  is fixed for a particular engine order excitation, the tuning order  $\tilde{n}$  depends on the model parameters  $\alpha$ ,  $\delta$ , and  $\gamma$  (these are prescribed by design), and the additional choice for the dimensionless absorber mass  $\mu$  sets the critical tuning order  $\hat{n}(\tilde{n})$ . The tuning strategy employed here is to simply choose these parameters to optimally orient the line  $\tilde{n}\sigma$  (and hence  $\hat{n}\sigma$ ) relative to  $n\sigma$  in the frequency- $\sigma$  plane. This in turn sets the asymptotic behavior of the system natural frequencies  $\bar{\omega}_{1,2}^{(i)}$  and hence prescribes the system resonance structure. It is clear that by choosing  $\tilde{n}\sigma = n\sigma$  (this corresponds to zero detuning) there will be no crossings of the order line  $n\sigma$  and the natural frequency loci  $\bar{\omega}_{1,2}^{(i)}(\sigma)$ , and hence there will be no system resonances over the full range of possible rotor speeds. However, slight errors in this tuning can introduce a resonance, and therefore such a design is not robust. One can more generally avoid resonances by choosing parameters such that  $\tilde{n} \leq n < \hat{n}(\tilde{n})$ . This is clear from the large- $\sigma$  asymptotic behavior of  $\bar{\omega}_2^{(i)}$ , and specifically from the inset of Fig. 3a. The existence of this finite, but narrow, tuning range allows one to design an absorber system with some level of robustness to uncertainties.

The arguments described above are developed in detail in the next section using the steady-state system response of Section 3.2, and in the context of absorber detuning in Section 4.2.

#### 4.1 Exact Tuning

It is customary to introduce the tuning order  $\tilde{n}$  as one of the absorber parameters, and this is done in the present study via the substitution

$$\gamma = \frac{\alpha + \delta}{\tilde{n}^2}, \quad (42)$$

thereby replacing  $\gamma$  with  $\tilde{n}$  in the formulation. With zero system damping, i.e.,  $\xi_a = \xi_b = \xi_c = 0$ , and after some simplification, the steady-state response described by Eq. (37) can be reduced to

$$\begin{bmatrix} x_i^{\text{ss}}(\tau) \\ y_i^{\text{ss}}(\tau) \end{bmatrix} = \begin{bmatrix} X \\ Y \end{bmatrix} e^{j\phi_i} e^{jn\sigma\tau}, \quad i \in \mathcal{N} \quad (43)$$

where

$$\left. \begin{aligned} X &= \frac{f\tilde{n}^2(n^2 - \tilde{n}^2)}{\Gamma} \\ Y &= -\frac{f\tilde{n}^2\left(\frac{\delta}{\alpha}(n^2 - \tilde{n}^2) + n^2(1 + \tilde{n}^2)\right)}{\left(1 + \frac{\delta}{\alpha}\right)\Gamma} \end{aligned} \right\} \quad (44)$$

are the blade and absorber steady-state response amplitudes and

$$\begin{aligned}\Gamma = & \mu\alpha^2(1 + \tilde{n}^2)^2 n^2 \sigma^2 + \tilde{n}^2(n^2 - \tilde{n}^2) \\ & + (n^2 - \tilde{n}^2) \left( \mu\alpha\delta(1 + \tilde{n}^2) - \tilde{n}^2(n^2 - \delta) \right) \sigma^2 \\ & + 2\nu^2 \tilde{n}^2(n^2 - \tilde{n}^2)(1 - \cos \varphi_{n+1}),\end{aligned}$$

where  $\varphi_i$  is defined by Eq. (3). The ideal, or *exact* absorber tuning follows by inspection of the first entry of Eq. (44) and is given by

$$\tilde{n} = n, \quad \text{or} \quad \bar{\omega}_{22} = \tilde{n}\sigma = n\sigma. \quad (45)$$

If the system is tuned according to Eq. (45) the blade and absorber amplitudes reduce to

$$\left. \begin{aligned} X &= 0 \\ Y &= -\frac{fn^2}{\mu\alpha^2\left(1 + \frac{\delta}{\alpha}\right)(1 + n^2)\sigma^2} \end{aligned} \right\}, \quad (\tilde{n} = n) \quad (46)$$

which shows that the blade vibrations can be eliminated completely. In this case the absorber amplitudes are inversely proportional to the mass ratio  $\mu$  and also to  $\alpha(\alpha + \delta)$ . It is therefore desirable to make the absorber masses large relative to the blade mass and to place them as close to the end of the blades as possible. In practice, however, there are limits on the size and makeup of the absorber masses (typically  $\mu$  is very small, on the order of  $10^{-2}$  to  $10^{-3}$ ) and their placement relative to the blades. The negative sign in  $Y$  implies that the absorbers oscillate out of phase with respect to the excitation. Physically, this means the absorbers exert forces on the blades that identically counter the action of the applied loading for all time and for all rotor speeds.<sup>12</sup>

#### 4.2 Absorber Detuning and the No-Resonance Gap

By implementing the absorber tuning given by Eq. (45) one is simply setting the natural frequency of the isolated absorbers to the excitation frequency, that is,  $\bar{\omega}_{22} = \tilde{n}\sigma = n\sigma$ , and the absorbers are said to be *exactly tuned*. Again, we emphasize that the said tuning is valid at all rotation speeds, a feature that is made possible by the structure of  $\bar{\omega}_{22}(\sigma) = \tilde{n}\sigma$ . However, any perturbation of the model or absorber parameters, due to in-service wear, environmental effects, and so on, will invariably destroy the exact tuning. To account for such

<sup>12</sup> These results remain valid even for varying rotor speeds, that is,  $\sigma = \sigma(\tau)$ , so long as variations in the rotor speed occur on a much longer time scale than the dynamics of the blades and absorbers.

effects, and to allow for intentionally detuned designs, we let

$$\tilde{n} = n(1 + \beta), \quad (47)$$

where  $\beta$  is a detuning parameter. Perfect, or exact tuning corresponds to  $\beta = 0$ , while undertuning (resp. overtuning) corresponds to  $\beta < 0$  (resp.  $\beta > 0$ ).

Figure 4 depicts the blade/absorber frequency response amplitude curves and also the natural frequency loci for a set of three representative detuning values. The corresponding tuning orders, detuning data, and the resonant rotor speeds are given in Table 3, along with data for exact absorber tuning. In these plots we take  $f = 0.01$  and use the parameters employed in Fig. 3c. The solid lines in the blade and absorber response curves show the response amplitudes as a function of rotor speed. The dashed lines in the blade frequency response curves correspond to the blade amplitudes when the absorbers are locked in their zero positions relative to the blades; these curves are used for reference to assess the dynamic effects of the absorbers.

Overtuning the absorbers (i.e., setting  $\beta > 0$ ) increases the slope  $\tilde{n}$  of  $\bar{\omega}_{22}(\sigma) = \tilde{n}\sigma$  relative to the engine order  $n$  in the frequency- $\sigma$  planes, and it is clear from Fig. 4a that a resonance of the in-phase mode corresponding to  $\bar{\omega}_1^{(n+1)}$  is guaranteed. For sufficiently large undertuning such that  $\beta < \beta_{\text{cr}} < 0$  (with  $\beta_{\text{cr}}$  defined below), the out-of-phase mode corresponding to  $\bar{\omega}_2^{(n+1)}$  is excited near resonance; an example of this situation is shown in Fig. 4c for  $\beta = -0.10$ . One of the more interesting findings of this study is that there are no system resonances for absorber tuning satisfying

$$\beta_{\text{cr}} < \beta \leq 0, \quad (48)$$

where  $\beta_{\text{cr}}$  is the *critical absorber undertuning* and is given by Eq. (B.2) of Appendix B. Zero (resp. critical) detuning, that is,  $\beta = 0$  (resp.  $\beta = \beta_{\text{cr}}$ ), corresponds to  $\tilde{n} = n$  (resp.  $\hat{n} = n$ ). An example of tuning within the *no-resonance gap* defined by Eq. (48) is shown in Fig. 4b for  $\beta = \beta_{\text{cr}}/2 = -0.00351$ , where  $\beta_{\text{cr}} = -0.00701$ . This case clearly demonstrates the effectiveness of properly tuned absorbers. The resonance that occurred at  $\sigma_{\text{res}} = 0.442$  when the absorbers are locked is completely eliminated, and the response amplitudes of the blades are reduced over the full range of possible rotor speeds.

It should be noted that impacts between the absorbers and the blades will occur whenever  $|y_i| = 1$ , or  $|\psi_i| = \psi_o$ , and this threshold can be identified in Fig. 4 by  $\log|Y| = 0$ . It appears from Fig. 4 that the absorbers may experience impacts over quite a large range of rotor speeds. Keep in mind, however, that the presence of damping will invariably reduce the blade/absorber amplitudes, and one cannot assess whether or not impacts will occur in its absence. The effects of damping will be described in a forthcoming paper [37], and the

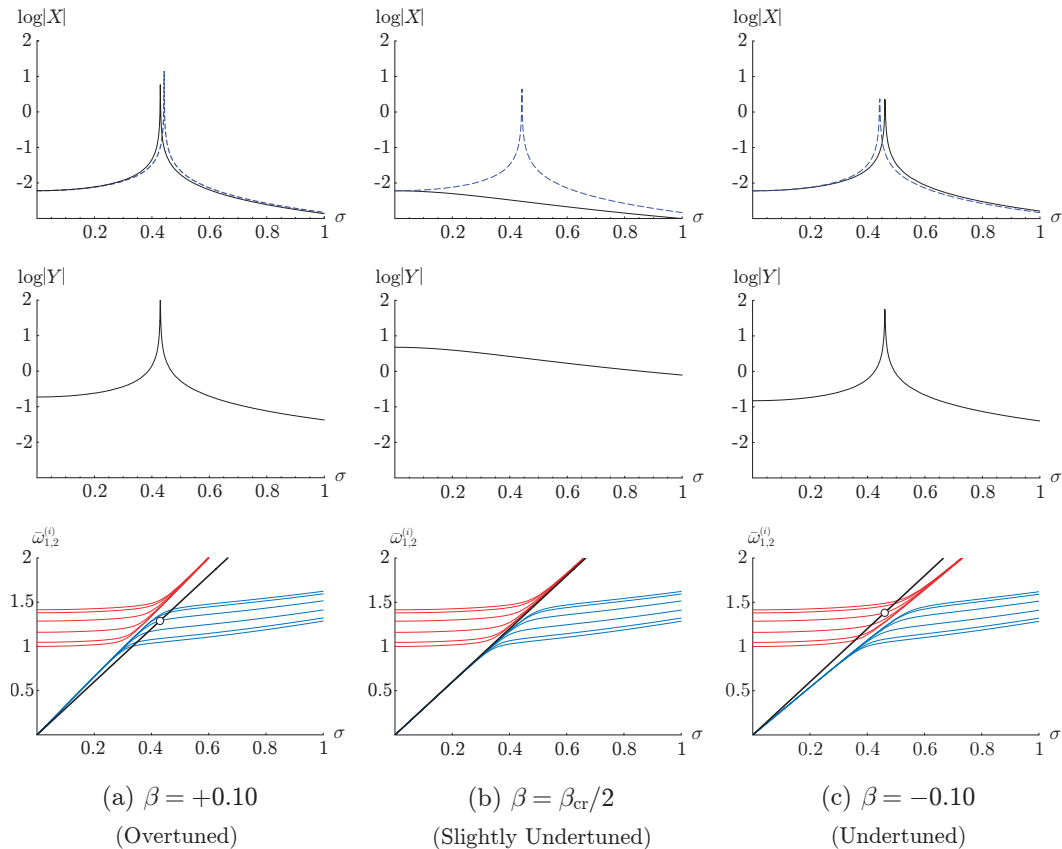


Fig. 4. Absorber and blade frequency response curves and Campbell diagrams for  $N = 10$ ,  $n = 3$ ,  $\alpha = 0.84$ ,  $\delta = 0.67$ ,  $\mu = 0.015$ ,  $\nu = 0.5$ ,  $f = 0.01$ , and zero damping: (a) +10% detuning ( $\beta = +0.10$ ); (b) -0.351% detuning ( $\beta = \beta_{cr}/2 = -0.00351$ ); (c) -10% detuning ( $\beta = -0.10$ ); (---) frequency response with the absorbers locked. The critical absorber detuning is  $\beta_{cr} = -0.00701$ . See Table 3 for the corresponding tuning order data and resonant rotor speeds  $\sigma_{res}$ .

impacting dynamics are treated in [15] for the case of a single blade/absorber combination. An investigation of the impact dynamics for the full cyclic system of Fig. 1a is left for future work.

Another way to visualize the no-resonance gap defined by Eq. (48) is to construct a plot of the rotor speeds  $\sigma_{res}$  corresponding to possible resonances versus the absorber detuning parameter  $\beta$ . Such a plot is shown in Fig. 5 for the same parameters used in Fig. 3 and Fig. 4. In this diagram, the no-resonance gap is identified by the region between the dotted lines corresponding to  $\beta = 0$  and  $\beta = \beta_{cr}$ , where  $\beta_{cr} = -0.00701$  for this case.

The extent of the no-resonance gap depends on the absorber parameters and the engine order, but is *independent* of the inter-blade coupling  $\nu$ . The sensitivity of the gap to variations in these parameters is indicated in Fig. 6, which follows from Eq. (B.2) in Appendix B. (A simpler approximate expression, which works quite well over a wide range of parameters, is described below.)

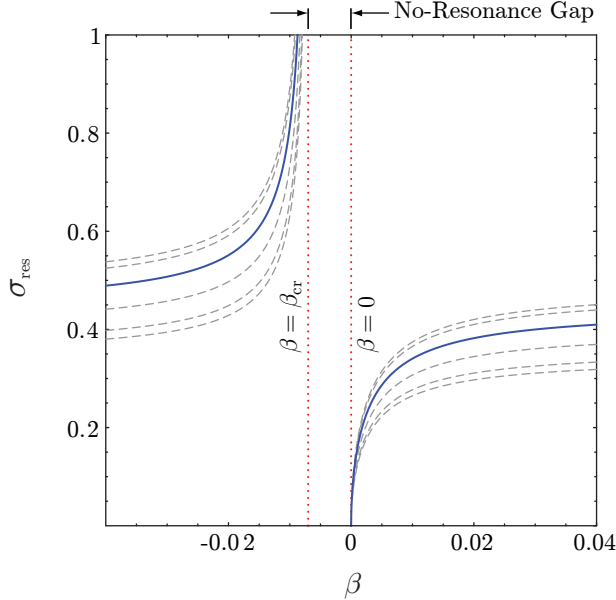


Fig. 5. Rotor speeds  $\sigma_{\text{res}}$  corresponding to possible resonances (—) and those that satisfy Eq. (41) (---) versus the absorber detuning  $\beta$  for  $N = 10$ ,  $n = 3$ ,  $\alpha = 0.84$ ,  $\delta = 0.67$ ,  $\mu = 0.015$ , and  $\nu = 0.50$ . The no-resonance gap is defined by  $\beta_{\text{cr}} < \beta \leq 0$ , where  $\beta_{\text{cr}} = -0.00701$ .

In all cases, the sensitivity is most pronounced for small engine orders and it decreases for increasing  $n$ . As shown in Fig. 6a (resp. Fig. 6b) the critical detuning  $\beta_{\text{cr}}$  exhibits near-linear (resp. -quadratic) behavior in terms of  $\mu$  (resp.  $\alpha$ ), and by inspection of Fig. 6c it is nearly independent of  $\delta$  for most engine orders ( $n > 2$ ). Note that  $\beta_{\text{cr}}$  vanishes (implying that the no-resonance gap vanishes) in the absence of the absorbers ( $\mu = 0$ ) or when the absorbers are attached to the periphery of the rotor ( $\alpha = 0$ ). This is consistent with intuition since zero-mass absorbers cannot provide the required loads to counter the action of the excitation on the blades. Also, if the absorber and blade pendulum attachment points coincide on the circumference of the rigid rotor, their dynamics become independent. It is clear, therefore, that both  $\mu$  and  $\alpha$  are coupling parameters in the sense that their departure from zero implies dynamic coupling between the blades and absorbers.

The parameter trends described above, and in particular those shown in Fig. 6a and Fig. 6b, motivate an expansion of  $\beta_{\text{cr}}$  in terms of  $\mu$  (resp.  $\alpha$ ) about  $\mu = 0$  (resp.  $\alpha = 0$ ) while keeping only linear (resp. quadratic) terms. Both expansions result in the simple approximation

$$\beta_{\text{cr}}^{\text{app}} = -\frac{(n^2 + 1)^2}{2n^2(n^2 - \delta)} \mu \alpha^2 + \mathcal{O}(\mu^2, \alpha^3), \quad (49)$$

which works quite well over a large range of realistic parameter values.

Based on the above analysis it is reasonable to choose  $\beta = \beta_{\text{cr}}/2$ , which is

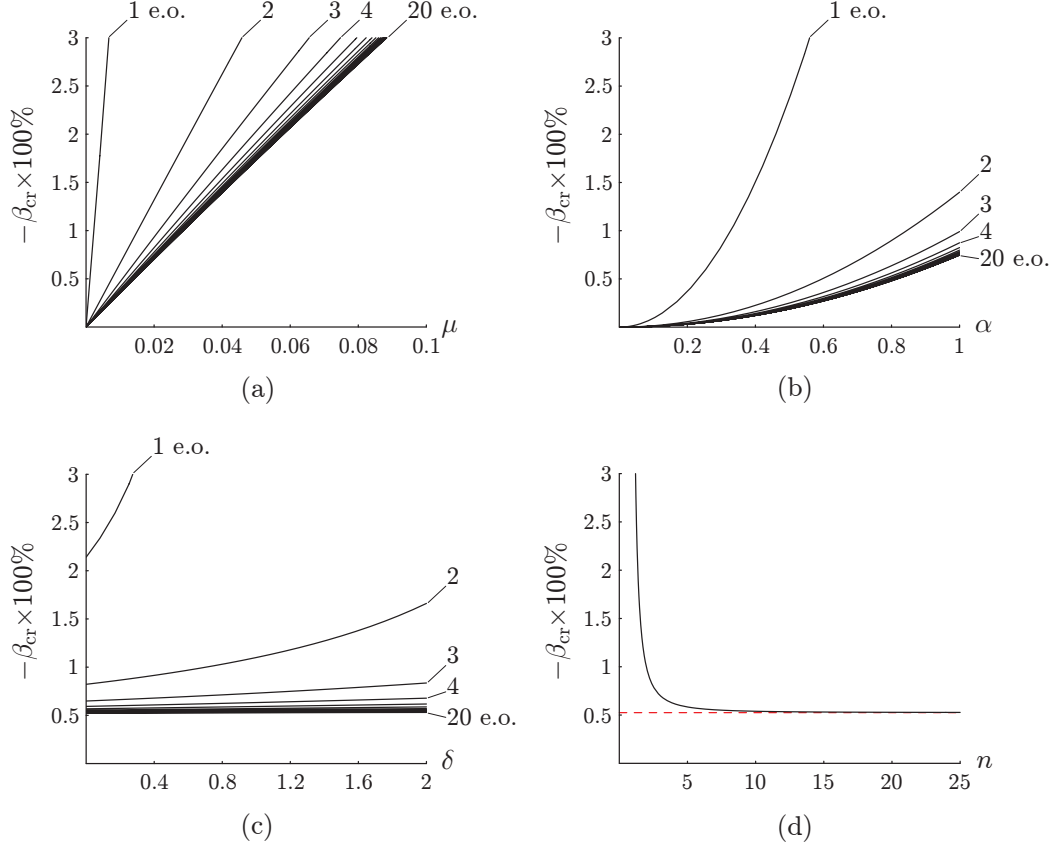


Fig. 6. Critical percent undertuning  $-\beta_{\text{cr}} \times 100\%$  of the absorbers versus (a) the dimensionless absorber mass  $\mu$  (with  $\alpha = 0.84$  and  $\delta = 0.67$ ), (b) the dimensionless distance from blade base to absorber base point  $\alpha$  (with  $\delta = 0.67$  and  $\mu = 0.015$ ), (c) the dimensionless radius of rotor disk  $\delta$  (with  $\alpha = 0.84$  and  $\mu = 0.015$ ), and (d) the engine order  $n$  (with  $\alpha = 0.84$ ,  $\delta = 0.67$ , and  $\mu = 0.015$ ). The dashed line in (d) corresponds to the large- $n$  approximation of  $\beta_{\text{cr}}$  given by Eq. (B.3) in Appendix B.

simply the average of the exact and critical detuning. Then Eq. (47) becomes

$$\tilde{n} = n \left( 1 + \frac{\beta_{\text{cr}}}{2} \right) \quad (50)$$

and the engine order  $n$  is very close to (but not exactly) the average of  $\hat{n}(\tilde{n})$  and  $\tilde{n}$ . Such a tuning strategy, which is used in the example shown in Fig. 4b, guarantees (in the absence of damping) no system resonances and it offers good robustness to parameter and model uncertainties. If one has detailed information about the nature of the model uncertainties, such information could be used to provide a more optimal tuning.

## 5 Conclusions and Directions for Future Work

An implementation of order-tuned vibration absorbers to a cyclically symmetric bladed disk model has been investigated. A standard change of coordinates based on the cyclic symmetry of the system was employed to reduce the governing  $2N$  equations of motion to a set of  $N$ , reduced-order equations, and absorber tuning strategies were formulated based on these equations. It was shown that ideal, or exact absorber tuning—where the absorber tuning order is chosen to match the order of the excitation—completely eliminates the system resonances and (in the absence of damping) results in zero-amplitude steady-state blade vibrations over all rotor speeds. Such a tuning scheme, however, is susceptible to the effects of parameter uncertainties. An important finding of this study is that, in addition to the exact tuning, there exists a *range* of absorber undertuning values for which there are no system resonances. Therefore, a practical tuning strategy might involve intentionally detuning the absorbers within this *no-resonance gap*. This approach offers a more robust design against system resonances, but at the expense of some residual steady-state blade vibrations (which will occur in any case, due to other effects, not modeled herein). As is the case with classical absorber theory [5, 6], the presence of damping will invariably alter this picture. However, for these order-tuned absorbers, it is desired to have small damping, since they remain tuned over all operating conditions. The effects of damping on the effectiveness of the absorbers will be considered in a future paper [37].

The absorber tuning scheme presented here is based on linear vibrations of an ideal undamped system with identical blades and identical absorbers. The results offer a basic understanding of the effectiveness of order-tuned vibration absorbers on the forced response of a bladed disk, and serve as a first step to the investigation of more realistic models. Some topics for future work include the inclusion of general-path absorbers that will allow for large amplitude (nonlinear) responses [38, 39], the effects of damping [37], and multi-DOF blade models [16] with, for example, nonlinear effects, imperfections [40], and intentional mistuning [41, 42].

### Acknowledgements

This work was supported by grant CMS-0408866 from the National Science Foundation. SWS is grateful to the Departments of Mechanical Engineering at the University of Michigan and the University of California - Santa Barbara for visiting appointments during which this work was initiated. BJO is grateful to Jeff Rhoads of Michigan State University and Matt Castanier of the University of Michigan for helpful discussions.

## A Mathematical Preliminaries

This appendix reviews some mathematical topics that may not be familiar to the reader, including the Kronecker product, the Fourier matrix, and the theory of circulant matrices. Special attention is given to the diagonalization of circulants and block circulants, the results of which are used to decouple the governing equations of motion given by Eq. (16) and Eq. (9), respectively. A detailed account of the theory of circulant matrices can be found in the work by Davis [23]; proofs of many of the results are detailed in [16, 22] from a linear vibrations viewpoint. See also [17, 18, 21] for further insight into uncoupling the dynamic equations of motion for periodic structures.

### A.1 The Kronecker Product

Let the matrices  $\mathbf{A}$  and  $\mathbf{B}$  be  $m \times n$  and  $p \times q$ , respectively. Then the Kronecker (direct) product of  $\mathbf{A}$  and  $\mathbf{B}$  is the  $mp \times nq$  matrix

$$\mathbf{A} \otimes \mathbf{B} = \begin{bmatrix} a_{11}\mathbf{B} & a_{12}\mathbf{B} & \cdots & a_{1n}\mathbf{B} \\ a_{21}\mathbf{B} & a_{22}\mathbf{B} & \cdots & a_{2n}\mathbf{B} \\ \vdots & \vdots & \ddots & \vdots \\ a_{m1}\mathbf{B} & a_{m2}\mathbf{B} & \cdots & a_{mn}\mathbf{B} \end{bmatrix}. \quad (\text{A.1})$$

Some selected useful properties of the Kronecker product are the following:

- (1) If  $\mathbf{A}$ ,  $\mathbf{B}$ ,  $\mathbf{C}$ , and  $\mathbf{D}$  are square matrices such that  $\mathbf{AC}$  and  $\mathbf{BD}$  exist, then  $(\mathbf{A} \otimes \mathbf{B})(\mathbf{C} \otimes \mathbf{D}) = (\mathbf{AC}) \otimes (\mathbf{BD})$ .
- (2) If  $\mathbf{A}$  and  $\mathbf{B}$  are invertible matrices, then  $(\mathbf{A} \otimes \mathbf{B})^{-1} = \mathbf{A}^{-1} \otimes \mathbf{B}^{-1}$ .
- (3) If  $\mathbf{A}$  and  $\mathbf{B}$  are square matrices, then  $(\mathbf{A} \otimes \mathbf{B})^{\mathcal{H}} = \mathbf{A}^{\mathcal{H}} \otimes \mathbf{B}^{\mathcal{H}}$ .

Here,  $(\cdot)^{\mathcal{H}} = (\bar{\cdot})^T$  denotes the conjugate transpose.

### A.2 The Fourier Matrix

The  $N \times N$  complex Fourier matrix is defined as

$$\mathbf{E}_N = [e_{ik}]; \quad e_{ik} = \frac{1}{\sqrt{N}} w^{(i-1)(k-1)}, \quad i, k = 1, \dots, N \quad (\text{A.2})$$

where  $w = e^{\frac{2j\pi}{N}}$  is the primitive  $N^{\text{th}}$  root of unity, and  $j = \sqrt{-1}$ . When the dimension of  $\mathbf{E}_N$  is clear, the subscript  $N$  will be omitted.

It is shown subsequently that all circulant matrices share the same linearly independent eigenvectors, the elements of which compose the  $N$  columns (or rows) of  $\mathbf{E}$ . They are denoted by the column vectors

$$\mathbf{e}_i = \frac{1}{\sqrt{N}} \left( 1, w^{(i-1)}, w^{2(i-1)}, \dots, w^{(N-1)(i-1)} \right)^T, \quad i = 1, \dots, N. \quad (\text{A.3})$$

Equation (A.3) can also be written in terms of  $\varphi_i$ , which is given by Eq. (3), by noting that  $e^{j\varphi_i} = w^{(i-1)}$ .

An important property of the Fourier matrix is that it is unitary and, therefore,

$$\mathbf{E}^H \mathbf{E} = \mathbf{E} \mathbf{E}^H = \mathbf{I}, \quad (\text{A.4})$$

where  $\mathbf{I}$  is the identity matrix. Finally, if  $\mathbf{E}$  is unitary then so are the matrices  $\mathbf{E}^H$ ,  $\mathbf{E} \otimes \mathbf{I}$ , and  $(\mathbf{E} \otimes \mathbf{I})^H = \mathbf{E}^H \otimes \mathbf{I}$ .

### A.3 Circulant Matrices

An  $N \times N$  *circulant matrix* (or *circulant* for short) is formed from an  $N$ -vector by cyclically permuting its entries, and is of the form

$$\mathbf{C} = \begin{bmatrix} c_1 & c_2 & \cdots & c_N \\ c_N & c_1 & \cdots & c_{N-1} \\ \vdots & \vdots & \ddots & \vdots \\ c_2 & c_3 & \cdots & c_1 \end{bmatrix}. \quad (\text{A.5})$$

Thus a circulant matrix is defined completely by an ordered set of *generating elements*  $c_1, c_2, \dots, c_N$ . It is convenient to define the *circulant operator*  $\text{circ}(\cdot)$  that takes as its argument these generating elements and results in the array given by Eq. (A.5), that is,

$$\mathbf{C} = \text{circ}(c_1, c_2, \dots, c_N). \quad (\text{A.6})$$

An  $NP \times NP$  *block circulant* matrix is defined similarly to Eq. (A.5) and has the representation given by Eq. (A.6), where each entry  $c_k$  is replaced by the  $P \times P$  matrix  $\mathbf{C}_k$  for  $k = 1, \dots, N$ . The ordered set of matrices  $\mathbf{C}_1, \mathbf{C}_2, \dots, \mathbf{C}_N$  are referred to as its *generating matrices*.

#### A.4 Diagonalization of Circulants

Equation (A.5) can be diagonalized via the unitary (similarity) transformation

$$\mathbf{E}_N^{\mathcal{H}} \mathbf{C} \mathbf{E}_N = \begin{bmatrix} \lambda_1 & & 0 \\ & \lambda_2 & \\ 0 & & \ddots \\ & & & \lambda_N \end{bmatrix}, \quad (\text{A.7})$$

where

$$\lambda_i = \sum_{k=1}^N c_k w^{(k-1)(i-1)}, \quad i = 1, \dots, N. \quad (\text{A.8})$$

As a consequence, *all* circulant matrices share the same eigenvectors, which are given by Eq. (A.3). Their eigenvalues are given by Eq. (A.8) and depend on the generating elements  $c_1, c_2, \dots, c_N$ .

An  $NP \times NP$  block circulant matrix  $\mathbf{C}$  with  $P \times P$  blocks  $\mathbf{C}_k$  can be block diagonalized via the unitary (similarity) transformation

$$(\mathbf{E}_N^{\mathcal{H}} \otimes \mathbf{I}_P) \mathbf{C} (\mathbf{E}_N \otimes \mathbf{I}_P) = \begin{bmatrix} \mathbf{\Lambda}_1 & & \mathbf{0} \\ & \mathbf{\Lambda}_2 & \\ \mathbf{0} & & \ddots \\ & & & \mathbf{\Lambda}_N \end{bmatrix}, \quad (\text{A.9})$$

where  $\mathbf{0}$  and  $\mathbf{I}_P$  are the  $P \times P$  zero and identity matrices, respectively, and

$$\mathbf{\Lambda}_i = \sum_{k=1}^N \mathbf{C}_k w^{(k-1)(i-1)}, \quad i = 1, \dots, N. \quad (\text{A.10})$$

Note that  $(\mathbf{E}_N \otimes \mathbf{I}_P)^{\mathcal{H}} = (\mathbf{E}_N^{\mathcal{H}} \otimes \mathbf{I}_P)$ . Since Eq. (A.9) is a unitary transformation, it preserves the eigenvalues of  $\mathbf{C}$ . Hence its eigenvalues are the eigenvalues of the  $N$ ,  $P \times P$  matrices  $\mathbf{\Lambda}_i$ . If  $\mathbf{v}_i$  is an eigenvector of  $\mathbf{\Lambda}_i$  then the corresponding eigenvector of  $\mathbf{C}$  is  $\mathbf{e}_i \otimes \mathbf{v}_i$ .

## B The Critical Detuning and Tuning Order

The critical absorber tuning order  $\hat{n}$  is defined implicitly by Eq. (39) and represents the limiting slope of the natural frequencies  $\bar{\omega}_2^{(i)}$  in the frequency versus  $\sigma$  curves of Fig. 3. It is convenient to express  $\hat{n}$  in terms of the absorber

tuning order  $\tilde{n}$ , which is introduced via Eq. (42). Then

$$\hat{n}(\tilde{n}) = \sqrt{\frac{\hat{a}_1\mu + \hat{a}_0 + \sqrt{\hat{a}_1^2\mu^2 + \hat{b}_1\mu + \hat{b}_0^2}}{2\tilde{n}^2}}, \quad (\text{B.1})$$

where

$$\left. \begin{aligned} \hat{a}_0 &= \tilde{n}^2(\tilde{n}^2 + \delta) \\ \hat{b}_0 &= \tilde{n}^2(\tilde{n}^2 - \delta) \\ \hat{a}_1 &= \alpha^2(\tilde{n}^2 + 1)\left(\tilde{n}^2 + \frac{\delta}{\alpha} + 1\right) \\ \hat{b}_1 &= 2\alpha^2\tilde{n}^2(\tilde{n}^2 + 1)\left((\tilde{n}^2 + 1)(\tilde{n}^2 + \delta) - \frac{\delta}{\alpha}(\tilde{n}^2 - \delta)\right) \end{aligned} \right\}.$$

The critical absorber undertuning can be obtained by replacing  $\tilde{n}$  with  $n(1+\beta)$  in Eq. (B.1), setting  $\hat{n} = n$ , and then solving for  $\beta = \beta_{\text{cr}}$ . Then  $\beta_{\text{cr}}$  is given implicitly by

$$(1 + \beta_{\text{cr}})^2 = \frac{a_1\mu + c_0 + \sqrt{b_2\mu^2 + b_1\mu + c_0^2}}{c_1\mu + 2c_0}, \quad (\text{B.2})$$

where

$$\left. \begin{aligned} a_1 &= \alpha^2\left(\frac{\delta}{\alpha} - n^2\left(2 + \frac{\delta}{\alpha}\right)\right) \\ b_1 &= -2\alpha^2n^2(n^2 - \delta)(n^2 + 1)\left(2 + \frac{\delta}{\alpha}\right) \\ b_2 &= \alpha^2\delta^2(n^2 + 1)^2 \\ c_0 &= n^2(n^2 - \delta) \\ c_1 &= 2\alpha^2n^2\left(n^2 - \frac{\delta}{\alpha}\right) \end{aligned} \right\}.$$

Note that when  $\mu = 0$ , the right hand side of Eq. (B.2) is unity, which implies  $\beta_{\text{cr}} = 0$  (i.e., the no-resonance gap vanishes), and the same is true when  $\alpha = 0$  (in which case  $a_1 = b_1 = b_2 = c_1 \equiv 0$ , but  $c_0 \neq 0$ ).

It is clear from Fig. 6 that changes in  $\beta_{\text{cr}}$  due to parameter variations decrease for increasing engine order. In the limit as  $n \rightarrow \infty$  Eq. (B.2) reduces to

$$(1 + \beta_{\text{cr}})^2 = \frac{1}{1 + \alpha^2\mu}, \quad (n \rightarrow \infty) \quad (\text{B.3})$$

which is shown by the dashed line in Fig. 6d. It depends only on  $\alpha$  and  $\mu$  and approximates  $\beta_{\text{cr}}$  to within 3% of its limiting large- $n$  value for  $n \geq 10$ .

## References

- [1] D. J. Ewins, Vibration characteristics of bladed disc assemblies, *Journal of Mechanical Engineering Science* 15 (3) (1973) 165–186.
- [2] A. V. Srinivasan, Flutter and resonant vibration characteristics of engine blades, *Journal of Engineering for Gas Turbines and Power* 119 (4) (1997) 742–775.
- [3] A. V. Srinivasan, Vibrations of bladed-disk assemblies — a selected survey, *Journal of Vibration, Acoustics, Stress, and Reliability in Design* 106 (2) (1984) 165–168.
- [4] J. C. Slater, G. R. Minkiewicz, A. J. Blair, Forced response of bladed disk assemblies—a survey, *Shock and Vibration Digest* 31 (1) (1999) 17–24.
- [5] J. Ormondroyd, J. P. Den Hartog, The theory of dynamic vibration absorbers, *Transactions of the ASME* 50 (1928) A9–A22.
- [6] J. P. Den Hartog, *Mechanical Vibrations*, McGraw-Hill, New York, 1956.
- [7] J. P. Den Hartog, Tuned pendulums as torsional vibration eliminators, in: *Stephen Timoshenko 60th Anniversary Volume*, The Macmillan Company, New York, 1938, pp. 17–26.
- [8] W. Ker Wilson, *Practical Solutions of Torsional Vibration Problems*, 3rd Edition, Vol. IV, Chapman and Hall Ltd, London, 1968, Ch. XXX.
- [9] M. Wachs, The main rotor bifilar absorber and its effect on helicopter reliability/maintainability, *SAE Technical Paper Series* 730894.
- [10] M. Cook, Absolute absorption, *Car Craft Magazine* (1994) 75.
- [11] T. M. Nester, A. G. Haddow, S. W. Shaw, J. E. Brevick, V. J. Borowski., Vibration reduction in variable displacement engines using pendulum absorbers, in: *Proceedings of the SAE Noise and Vibration Conference and Exhibition*, no. 2003-01-1484, Traverse City, Michigan, 2003.
- [12] J. J. Hollkamp, R. L. Bagley, R. W. Gordon, A centrifugal pendulum absorber for rotating, hollow engine blades, *Journal of Sound and Vibration* 219 (3) (1999) 539–549.
- [13] Y. Wang, C. P. Chao, S. W. Shaw, Design of pendulum vibration absorbers for the attenuation of transverse vibrations in rotating beams, in: *Proceedings of the ASME 17th Biennial Conference on Mechanical Vibration and Noise*, no. DETC97/VIB-4182, Sacramento, California, 1997.
- [14] K. P. Duffy, R. L. Bagley, O. Mehmed, On a self-tuning impact vibration damper for rotating turbomachinery, in: *36th AIAA/ASME/SAE/ASEE Joint Propulsion Conference and Exhibit*, no. AIAA-2000-3100, Huntsville, Alabama, 2000.

- [15] S. W. Shaw, C. Pierre, The dynamic response of tuned impact absorbers for rotating flexible structures, *Journal of Computational and Nonlinear Dynamics* 1 (2006) 13–24.
- [16] G. S. Óttarsson, Dynamic modeling and vibration analysis of mistuned bladed disks, Ph.D. dissertation, University of Michigan, Ann Arbor, MI (1994).
- [17] L. F. Wagner, J. H. Griffin, Forced harmonic response of grouped blade systems: Part i—discrete theory, *Journal of Engineering for Gas Turbines and Power* 118 (1996) 130–136.
- [18] C. W. Cai, Y. K. Cheung, H. C. Chan, Uncoupling of dynamic equations for periodic structures, *Journal of Sound and Vibration* 139 (2) (1990) 253–263.
- [19] L. Meirovitch, *Principles and Techniques of Vibrations*, Prentice Hall, Upper Saddle River, 1997.
- [20] C. W. Cai, Y. K. Cheung, H. C. Chan, Dynamic response of infinite continuous beams subjected to a moving force—an exact method, *Journal of Sound and Vibration* 123 (3) (1988) 461–472.
- [21] I. Y. Shen, Vibration of rotationally periodic structures, *Journal of Sound and Vibration* 172 (4) (1994) 459–470.
- [22] B. J. Olson, Order-tuned vibration absorbers for systems with cyclic symmetry with applications to turbomachinery, Ph.D. dissertation (in preparation), Michigan State University, East Lansing, MI.
- [23] P. J. Davis, *Circulant Matrices*, 2nd Edition, John Wiley & Sons, New York, 1979.
- [24] P. W. Anderson, Absence of diffusion in certain random lattices, *Physical Review* 109 (5) (1958) 1492–1505.
- [25] C. H. Hodges, Confinement of vibration by structural irregularity, *Journal of Sound and Vibration* 82 (3) (1982) 411–424.
- [26] C. Pierre, E. H. Dowell, Localization of vibrations by structural irregularity, *Journal of Sound and Vibration* 114 (1987) 549–564.
- [27] D. S. Whitehead, Effect of mistuning on the vibration of turbomachine blades induced by wakes, *Journal of Mechanical Engineering Science* 8 (1) (1966) 15–21.
- [28] R. C. F. Dye, T. A. Henry, Vibration amplitudes of compressor blades resulting from scatter in blade natural frequencies, *Journal of Engineering for Power* 91 (1969) 182–188.
- [29] D. S. Whitehead, The maximum factor by which forced vibration of blades can increase due to mistuning, *Journal of Engineering for Gas Turbines and Power* 120 (1) (1998) 115–119.
- [30] D. J. Ewins, The effect of detuning upon the forced vibrations of bladed disks, *Journal of Sound and Vibration* 9 (1) (1969) 65–79.

- [31] J. C. MacBain, P. W. Whaley, Maximum resonant response of mistuned bladed disks, *Journal of Vibration, Acoustics, Stress, and Reliability in Design* 106 (2) (1984) 218–223.
- [32] B. J. Olson, S. W. Shaw, M. P. Castanier, C. Pierre, On the resonance structure of a rotating cyclic system under large-order traveling-wave excitation, in preparation.
- [33] D. L. Thomas, Dynamics of rotationally periodic structures, *International Journal for Numerical Methods in Engineering* 14 (1979) 81–102.
- [34] D. J. Ewins, A study of resonance coincidence in bladed discs, *Journal of Mechanical Engineering Science* 12 (5) (1970) 305–312.
- [35] N. C. Perkins, J. C. D. Mode, Comments on curve veering in eigenvalue problems, *Journal of Sound and Vibration* 106 (3) (1986) 451–463.
- [36] C. Pierre, Mode localization and eigenvalue loci veering phenomena in disordered structures, *Journal of Sound and Vibration* 126 (3) (1988) 485–502.
- [37] B. J. Olson, S. W. Shaw, C. Pierre, The effects of damping on the effectiveness of vibration absorbers for a cyclic rotating flexible structure.
- [38] A. S. Alsuwaiyan, S. W. Shaw, Performance and dynamic stability of general-path centrifugal pendulum vibration absorbers, *Journal of Sound and Vibration* 252 (5) (2002) 791–815.
- [39] S. W. Shaw, A. Alsuwaiyan, Torsional vibration reduction using passive nonlinear absorbers, in: *Proceedings of the SPIE Conference on Smart Structures*, Newport Beach, California, 2000.
- [40] S. T. Wei, C. Pierre, Localization phenomena in mistuned assemblies with cyclic symmetry part ii: Forced vibrations, *Journal of Vibration, Acoustics, Stress, and Reliability in Design* 110 (1988) 439–449.
- [41] M. P. Castanier, C. Pierre, Consideration on the benefits of intentional blade mistuning for the forced response of turbomachinery rotors, *Analysis and Design Issues for Modern Aerospace Vehicles* 55 (1997) 419–425.
- [42] M. P. Castanier, C. Pierre, Using intentional mistuning in the design of turbomachinery rotors, *AIAA Journal* 40 (10) (2002) 2077–2086.